




Faculty of Science and Technology

## BACHELOR'S THESIS

<b>Study program/ Specialization:</b>  Computer Science	Spring Semester 2022  Open access
<b>Writers:</b> Einar Holst-Larsen	 Writer's Signature
<b>Faculty Supervisor:</b> Morteza Esmaeili	
<b>Thesis title:</b> Magnetic Resonance: Simulating Spin Magnetization	
<b>Credits (ECTS):</b> 20	
<b>Key Words</b> <ul style="list-style-type: none"><li>• Magnetic Resonance Imaging</li><li>• Simulations</li><li>• Bloch equations</li></ul>	Pages: 49 +enclosure: 0 Stavanger May 15, 2022



Faculty of Science and Technology  
Department of Electrical Engineering and Computer Science

# Magnetic Resonance: Simulating Spin Magnetization

Bachelor's Thesis in Computer Science  
by

Einar Holst-Larsen

Internal Supervisor  
Morteza Esmaeili

May 15, 2022

## Abstract

Magnetic resonance (MR) imaging modalities provide non-invasive and non-harmful *in vivo* imaging tools for clinical investigations. The standard clinical MR protocols used in brain examinations comprise several anatomical imaging techniques. This work describes the principal physics behind some common MR contrasts and their applications in clinical routines and neuroscience. The excellent contrast derived from the brain's anatomy partly relies on water's hydrogen nuclei ("spins") relaxation time differences in tissues. Also, the project provides a simulation platform to demonstrate the spin behavior in a strong static magnetic field, reflecting the relaxation parameters. The model simulation and spin dynamics will be derived from the Bloch equations.

## **Acknowledgements**

I am greatly in dept to the faculty supervisor Morteza Esmaili for his counseling. He has been very patient with teaching me difficult subject. His availability and constructive inputs have been very beneficial to the writing.

# Contents

<b>Abstract</b>	<b>4</b>
<b>Acknowledgements</b>	<b>4</b>
<b>1 Introduction</b>	<b>5</b>
1.1 What is MRI?	5
1.2 History	6
1.3 Goals and Inspiration	7
1.4 Outline	7
<b>2 Background</b>	<b>8</b>
2.1 MRI System	8
2.2 Main Magnet	11
2.3 Radiofrequency Coils	13
2.3.1 Receive-only Coils	14
2.4 Gradient Coils	15
<b>3 Basics of Magnetic Resonance Imaging</b>	<b>18</b>
3.1 Classical Description	18
3.2 Nuclei Behavior in a Magnetic Field	20
3.3 Magnetization	22
3.4 Excitation	23
3.5 T2 Relaxation	24
3.6 T1 Relaxation	25
3.7 Image Acquisition	26
3.7.1 Slice Selection	26
3.7.2 Frequency Encoding	27
3.7.3 Phase Encoding	28
3.8 Spin Echo and Gradient Echo Sequences	29
3.9 Contrast in MRI	30
3.10 T1 Weighting	31
3.11 T2 Weighting	31
<b>4 Bloch Simulation</b>	<b>33</b>
4.1 The Bloch Equation	33
4.1.1 Frame of Reference	33
4.2 Simulations	34
4.2.1 Simulation 1 - 90 degree pulse	34
4.2.2 Simulation 2 - T2 Relaxation	36
4.2.3 Simulation 3 - T1 Relaxation	38
4.2.4 Simulation 4 - T1 and T2 Relaxation in grey and white matter	40
<b>5 Conclusion</b>	<b>43</b>

## 1 Introduction

This work provides an overview of some technical aspects and principles of Magnetic Resonance Imaging (MRI) systems, brief basics of magnetic resonance (MR) physics, and spin behavior simulation when placed in a strong magnetic field. Also, we address an example of a critical clinical application of MRI in diagnostic imaging and treatment evaluations. Furthermore, the thesis partly describes the history of the MR phenomena discovery.

### 1.1 What is MRI?

MRI is a non-invasive and non-ionizing imaging technique that provides *in vivo* (in a living organism) imaging of tissues in the human body. This technology employs computer-generated radio waves and strong magnetic fields to provide detailed images of areas inside the body. MRI plays a vital role in clinical imaging with extensive applications in disease and injury diagnosis to treatment monitoring and assessments. MRI machines can best detect damages, lesions, and pathology in soft tissues, such as the central nervous system (CNS), muscles, and tendons, viable for athletes struggling with injuries or patients with brain or internal organ diseases. The fact that the MRI system only deals with magnets and radiofrequency means that the procedures in MR techniques are radiation- and ionizing-free, rendering it completely safe to use. As the system is non-ionizing, patients can be examined longitudinally and frequently, and thus MRI provides more flexible treatment planning to follow up patient's status.

Three-dimensional (3D) MR images can be obtained from selective areas of the human body, which provides detailed pictures of the anatomical and structural of the organ, as also functional and metabolic information. An important application and prominent features of MRI technologies are multimodal imaging abilities to analyze the brain. MRI is considered the golden standard in brain studying because of its outstanding performance in soft tissues and ability to detect anomalies. Below is an example of an image with an axial (top-down/transverse) view, acquired at the first diagnostic session, of a patient who started feeling pain in the head. The patient received pain medication, but the pain did not go away. After a while, the patient had MR images taken of the body, only to find a tumor in the brain. The doctors gave a diagnosis of cancer that was a type of astrocytoma as seen in **[Figure 1]**. Astrocytoma is a type of cancer that begins in cells called astrocytes that support nerve cells in the CNS.

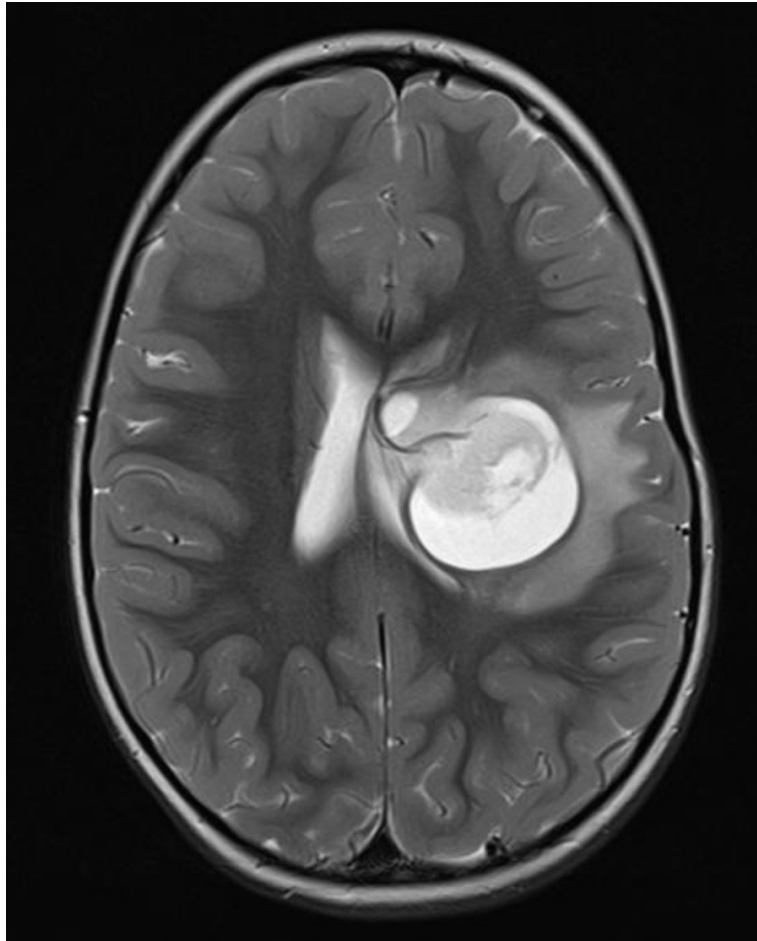


**Figure 1:** The astrocytoma lesion appears as the white area in the middle of the image of the patient's brain. Case courtesy of Dr Jones, J., *Supratentorial pilocytic astrocytoma*. Case study, Radiopaedia.org[1].

The above example is the pinnacle of lifesaving with MRI. The radiologists who analyzed these images delivered diagnostic reports to doctor specialists, neuroncologists, and neurosurgeons for further clinical procedures. They subsequently made a treatment plan for the patient to undergo standard care at the hospital, including surgery and chemotherapy. This patient was followed up and subjected to several post-surgical MRI examinations and ultimately survived. This shows how the MR technique can classify applications and lead to treatments, recovery, and survival. It shows the importance of why almost every hospital and many clinics wish to have at least one MRI system in their radiology department.

## 1.2 History

Before the first image of a human body part was produced by Sir Peter Mansfield and Paul Lauterbur in 1977[2], the magnetic resonance phenomena was first discovered in 1946 by the American physicist Edward Purcell (1912-1977) and the Swiss physicist Felix Bloch (1905-1983)[3]. Ever since then, it has been known that the physics of MRI can be explained in two ways - classical and quantum mechanical. Even though the fundamental principles of magnetic resonance are rooted in quantum mechanics, all concepts within MRI, especially those revolving around human tissue, are thoroughly described and can be understood well by using classical terms[4].

Felix Bloch classically explained the MR phenomenon with torque, flux lines, and induction measurements. The same kind of terms one would use to describe electromotors or transformers

- "classical" objects where magnetic field and energy distribution, and directions are described[5]. Purcell used quantum mechanical theories, in which spin orientation is quantized, has energy levels, and where the system is investigated through the absorption of energy from radio waves. Purcell's theories become more vital when describing the most advanced MR experiments.

Moreover, the motivation for the clinical use of MRI was to overcome the barriers of X-ray imaging, first used in the 1890s by the physicist Wilhelm Röntgen. While x-ray was mainly used to check for fractures in bone, it uses radiation; thus, the risk for cancer occurs. Also, x-ray imaging requires manual input for every two-dimensional image, while MRI automatically provides a complete 3D overview of the area. The techniques in MRI also play a critical role in the collaboration and interaction between doctors and computer scientists, introducing new ways of thinking and new procedures when it comes to a computer's role in medicine.

### 1.3 Goals and Inspiration

The use of clinical MRI in diagnosing disease and injuries is essential for people's health. The complicated systems used in MRI show how physics, computer science, and biology can work together to help hospitals and clinics. Some aspects of these subjects will be highlighted in this thesis.

This thesis shall describe the principle physics behind the MR contrasts and their applications in clinical routines and neurosciences for the brain.

It is assumed that the reader has prior knowledge in physics and mathematics subjects alike an engineering student of Bachelor level. The project aims to provide the reader with good knowledge about how the MR signal and magnetization develop from nuclear interaction with magnetic fields. The project should also be a simulation platform to help demonstrate the spin behavior of nuclei in a strong static magnetic field, reflecting the relaxation parameters. The model simulation and spin dynamics will be derived from the Bloch equations.

### 1.4 Outline

In summary, the following contributions are made in this thesis:

**Chapter 1** - Introduction and presentation of the MRI theme and motivation

**Chapter 2** - An overview of the MRI system, and how the parts and compartments cooperate

**Chapter 3** - General physics and MRI theory

**Chapter 4** - Simulations of the change in magnetization, following the Bloch equations

**Chapter 5** - Conclusion



## 2 Background

MRI machines use the physics of magnetization and radio waves which interact with nuclei in the tissue. The nuclei are forced into a state where they transmit signals which are then detected and interpreted by a computer in such a way that it produces gray-scaled images of the area of interest in the body. This chapter presents background related to MRI systems, MR physics, and Bloch simulations. We start by giving the core elements and parts of the MRI system. Further, we introduce the basic principles of spin behaviors in a static magnetic field.

MRI generates images based on protons in water and fat/lipid. MRI has several advantages over imaging modalities, particularly in using multiple pulse sequence programs that provide various tissue contrast. MR pulse sequences can be tailored by either operator during protocol planning or the physicist according to the clinician's needs to highlight a vast array of abnormalities in the study of organs. With access to a higher magnetic field, MRI systems can generate high-quality structural and anatomical images of the brain with sub-millimeter spatial resolution and even much better contrast of the distinction between tissue compartments such as white and gray matter in the brain. MRI may not be superior for all imaging applications. For instance, lung imaging can be more difficult to investigate with MRI than images acquired by computed tomography system as air cavities cause a sort of artifact in MR images and reduce signal intensity from the targeted tissues. Nevertheless, several studies have developed pulse sequences to improve lung MRI.

### 2.1 MRI System

MRI systems consist of several parts usually split into three rooms: examination room, technical room, and control room. The examination room contains the main magnet, patient table, enclosures, coil cabinets, and support footings. It is vital that none of the objects in this room can be influenced by the magnetic field. This room is shielded from radiofrequency (RF) waves to confine the magnetic field induced inside the room. It's also acoustically shielded to dampen the noise generated by the MRI machine. An MRI system and its main parts inside the examination room are shown in [Figure 2].

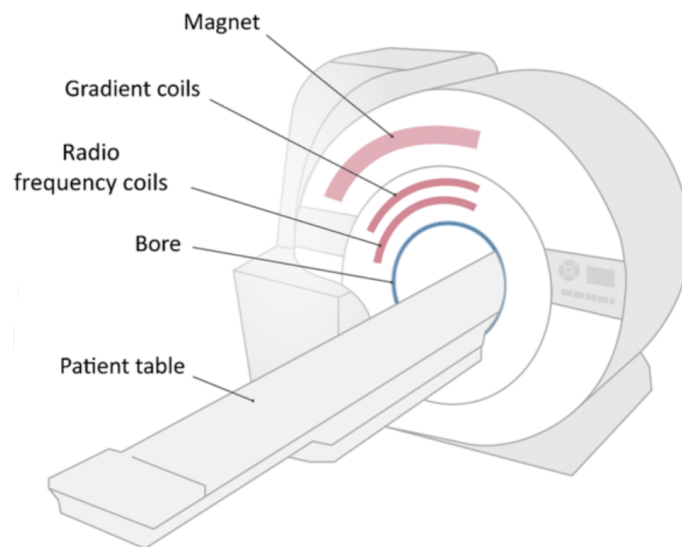


**Figure 2:** Example of an MRI system inside the examination room. From the outer to inner layers of the magnet: the main magnet, the gradient coils, the RF coils, the bore where the patient lies in examination and the magnetic field is the strongest, and a sample table in which the patient is placed onto before being rolled into the bore. Springer Nature journal content, brought to you courtesy of Springer Nature Customer Service Center GmbH[6].

The technical room is adjacent to the examination room and consists of several controlling cabinets such as RF amplifiers, gradient coils, helium pumps, and data acquisition and processing units. The power cabinet, water pump for cooling, and other electrical equipment are also located in this room. The main components of the room can be seen in [Figure 3].

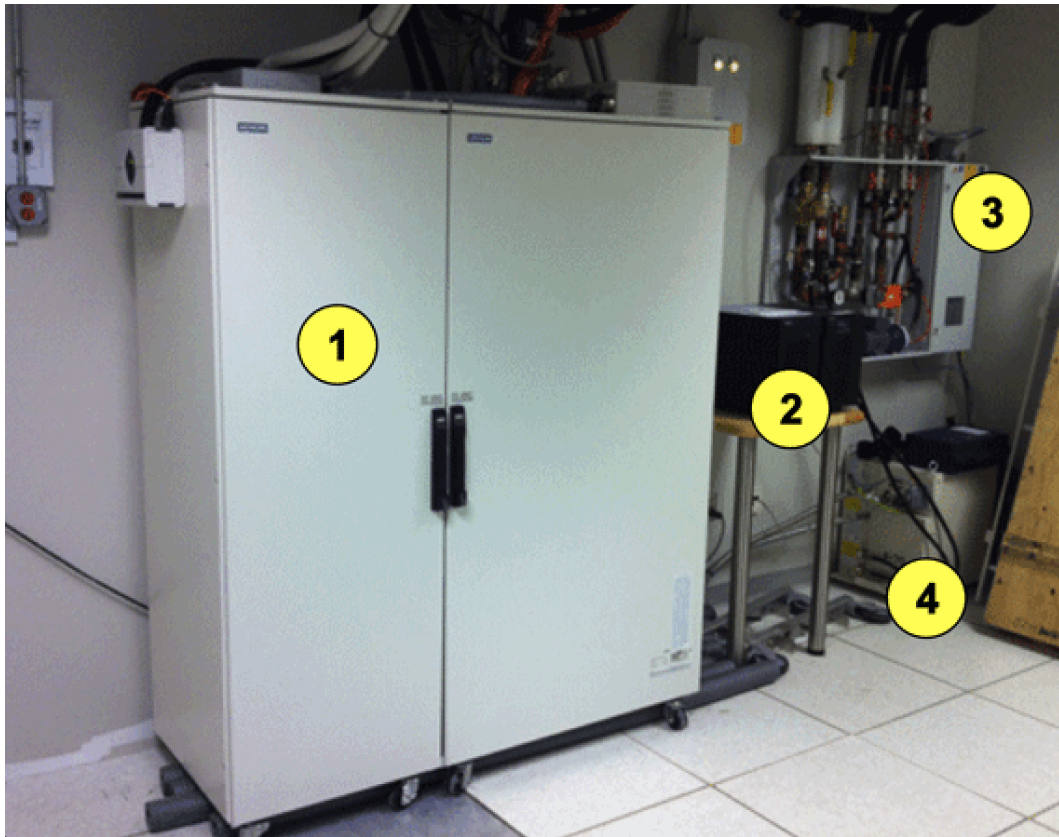


**Figure 3:** Number 1 showing a cabinet containing RF amplifiers that control the RF pulse transmission and reception, and power for the gradient coils. Number 2 is the general power supply. Number 3 is the water pump for cooling. Number 4 is the helium pump that pumps helium through the machine as a coolant. Courtesy of Allen D. Elster, MRIquestions.com[7].

The control room contains an operator console, communication devices, an electrocardiography (ECG) and oxygen monitoring screens, and computer equipment that controls the scanner. The MR operator can monitor the examination room through an RF-shielded window. A safety door separates these two rooms where a specific safety aspect is regulated for which restricting the materials allowed to the examination room. This is very important as the magnetic field inside the examination room is so powerful that no materials susceptible to magnetism can be out of control. The magnet has the power to pull objects with a power that is very dangerous if there are people nearby - an example of safety risk is provided in [Figure 4].



**Figure 4:** A picture showing a metal stool that has flown through the air into the bore. Photo by Moriel NessAiver via The New York Times[8].

## 2.2 Main Magnet

The main magnet is a set of coils wrapped around the bore inside the scanner. These coils are sets of current-carrying wires, which, according to Faraday's law of induction, induce a magnetic field. In the case of the coils in the main magnet, the magnetic field is induced on the inside of the coils, in a direction according to Maxwell's right-hand rule. By curling fingers and pointing the thumb upwards, the direction of the magnetic field points in the direction of the thumb [Figure 5]. The magnetic field in an MRI magnet is highly homogeneous, and of over ten thousand times the strength of the Earth's natural magnetic field. When a magnetic field is considered homogeneous, it has a constant magnitude and direction over the desired space. The importance of homogeneity in MRI will be highlighted in chapter 3.

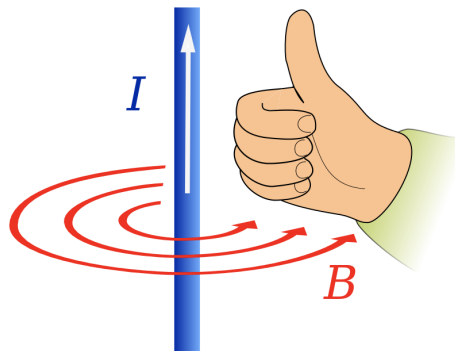


**Figure 5:** Showcase of Maxwell's right hand rule.  $I$  indicates the direction of the induced magnetic vector field coming from a current carried through the red  $B$ -lines. Image by Wikipedia contributor Jfmlero via Wikipedia[9].

From now on, the magnetic field induced by the main magnet can be referred to as  $B_0$ . A visualization of the magnetic field as seen induced by an MRI magnet is shown in [Figure 6]

below.

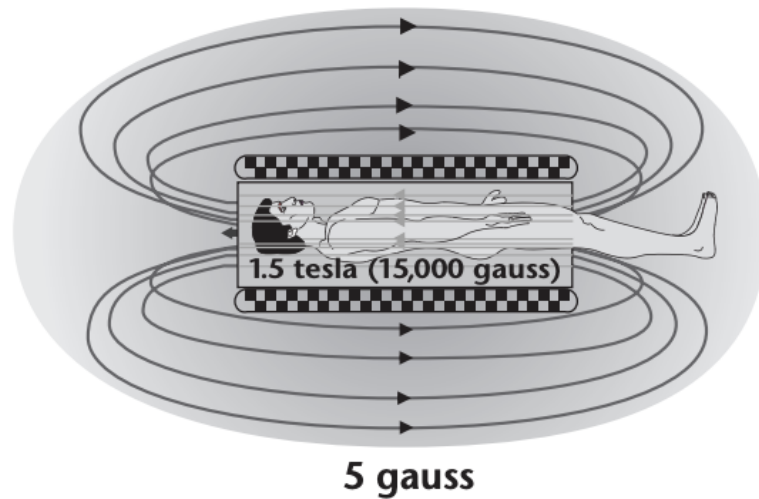


**Figure 6:** A slice of an MRI scanner with a magnetic field strength of 1.5 Tesla. The bars with dotted lines depict current-carrying coils which wrap around the bore, inducing the magnetic field. As seen in the figure, the field strength quickly diminishes with distance. Image from Perry Sprawls et al., an open-access resource[10].

The strength of  $B_0$  is measured by the Tesla (T) metric as seen in Figure 6 above. Tesla is a measure of field intensity, where 1T generates one newton per ampere per meter of conductor. 1 Tesla equals roughly 10000 Gauss. For scale, the magnetic field strength of the Earth's outer layers is approximately 25 Gauss. A typical clinical MRI scanner's strength is usually equipped with somewhere between 1.0 and 3.0T[11]. Recently, ultra-high-field 7 Tesla magnets have been put into practice in clinical settings, providing several improvements in neurological examinations. There can be several benefits associated with higher magnetic field strength. The ultra-high-field magnetic field strength provides a higher signal-to-noise ratio (SNR), thus enabling higher spatial resolution for structural imaging and more flexibility in designing pulse sequences for demanding functional imaging protocols. However, there are some technical challenges in providing a homogeneous magnetic field at an ultra-high-field as opposed to a standard 1 Tesla magnetic field strength.

Not all MRI examinations use one giant magnet. If a patient is to examine a knee or another small body part, portable smaller magnets can be used. In [Figure 7] below, a so-called knee coil and head coil are used for taking images of the head and knee. This is more convenient than using a big device as smaller machines have more homogeneous fields because the region's volume is smaller than the core size of the traditional magnets. Smaller magnets are also often used for animals and pre-clinical testing.



**Figure 7:** Figure (a) is a knee coil from Siemens[12]. Figure (b) is a head coil from Siemens[13]. Images credited to Siemens Historical Institute.

The most commonly used magnets are superconductive. Superconductivity is a property that certain materials possess in which there is no electrical resistance when a certain temperature - the critical temperature - is reached. This allows for current maintenance without voltage application. In other words, it does not need a power source to have a persistent electrical current. In MRI, these temperatures are reached by cooling the magnet down with helium. In essence, the superconductivity of the magnets makes it so the machine and magnet are never turned off.

### 2.3 Radiofrequency Coils

Radiofrequency (RF) coils are the "antennas" of the MRI system. The coils excite the magnetization by transmitting the RF power and receiving the signal from the spins (receive Rx-Coil). Transmit RF (Tx-Coil) waves emit magnetic field pulses (usually expressed by  $B_1$ , in the order of micro-Tesla) to rotate the net magnetization away from its alignment with the  $B_0$ . If the  $B_1$  power is adjusted for a  $90^\circ$  pulse, the rotation will be transverse precessing magnetization.

There are several types of RF coils. The innermost layer of the MRI machine consists of the RF coils (see [Figure 2]). Besides the inner-installed body coil inside the main magnet, several other types of RF coils are designed for different organs in the body. Most of the transmitter coils are birdcage designs like [Figure 8].

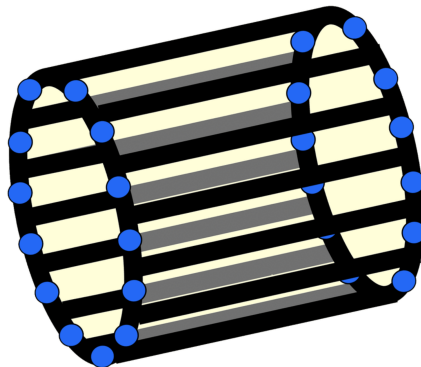


**Figure 8:** The birdcage RF coil design. The two circular conductive loops are the *end rings*. The loops are connected by conductive elements called *rungs*, numbering from 8 to 32. Courtesy of Allen D. Elster, MRIquestions.com[14].

Sinusoidal currents are sent through each rung with a different phase according to  $360^\circ/N$ , where  $N$  is the number of rungs. According to the antenna theory, with this current distribution with sinusoidal angular dependence on overall rungs, a resonance condition leads to a homogeneous magnetic field  $B_1$  created inside the birdcage. A depiction of how this works with six rungs is illustrated in [Figure 9].

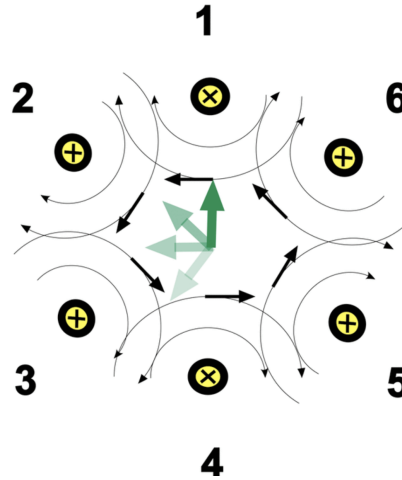


**Figure 9:** A hypothetical 6-rung birdcage coil where the current through each rung is directed inwards, marked with "x". As the peak of each of the sinusoidal currents hits, the maximum flux is induced. The boldest green arrows visualize this. First, the peak of rung 1 hits, then the peak of rung 2 hits, and so on. After the sinusoidal peak sequentially hits all rungs, a peak will hit rung 1 again, and the sequence will start over. The fluctuating magnet fields inside the coil are what induce  $B_1$ . Courtesy of Allen D. Elster, MRIquestions.com[14].

Plotting the resulting magnetic fields on the same grid will show an even pattern of waves. The sum of the fields will cancel each other out and thus create a homogeneous field [Figure 10].

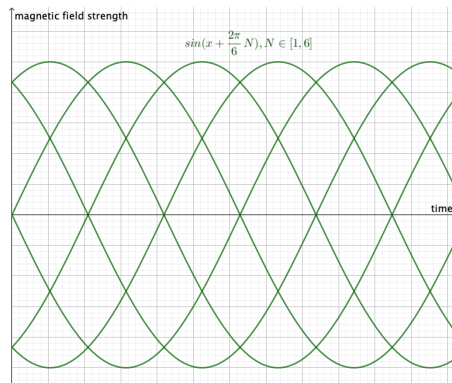


**Figure 10:** The magnetic field strength equation for each of the six rungs. The phase shift equals  $\frac{2\pi}{6}$  rad between each of them. All fields are summed together into one common field  $B_1$ , where the equation for this field is constant. Thus, the change  $\frac{dB_1}{dt}$  over time will always equal zero. If  $\frac{dB_1}{dt} = 0$ , it is homogeneous.

### 2.3.1 Receive-only Coils

The RF coils of the receive-only type are often surface coils. These are small coils shaped so they can be placed near the anatomical part imaged. The surface coils have a good signal-to-noise ratio

and are of simple design, often just a single loop of wire as in [Figure 11]. The surface coils allow for smaller voxels, which gives improved image resolution. A voxel is a pixel in three dimensions. In the case of MRI, it's a cube of tissue-related data with prefixed length, width, and height. A single MRI scan can consist of millions of voxels.

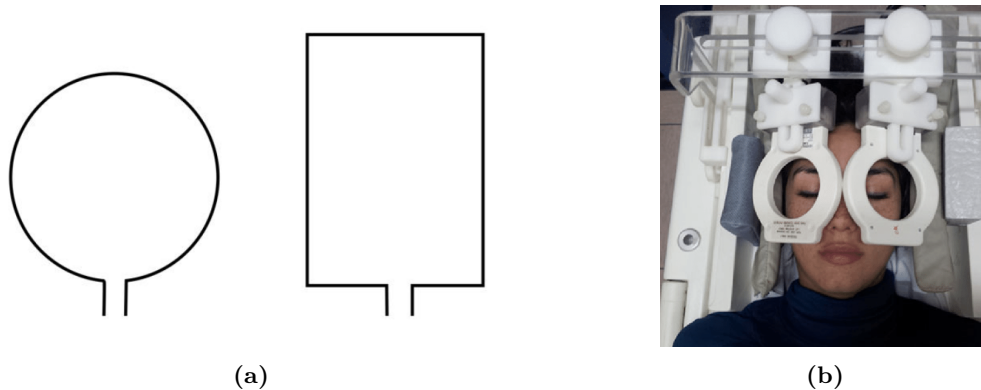


**Figure 11:** (a) Two simple drawings of surface coils. (b) An example of a clinical surface coil. Reprinted by permission from Springer Nature: Springer Nature, La radiologia medica. *Uveal melanoma: evaluation of extrascleral extension using thin-section MR of the eye with surface coils*, Tommaso Tartaglione et al., 2014[15].

## 2.4 Gradient Coils

In the middle layer of the are the *gradient coils*. These coils are either thin conductive sheets or loops of wire placed inside the bore. They alter and create variations in  $\mathbf{B}_0$  by producing smaller magnetic fields on the order of milli Tesla (mT). These field variations cause the properties of the nuclei in the tissue to change as a function of position, which makes it possible to locate the MR signal. The act of signal localization is called *spatial encoding*.

In nearly all MRI systems, three sets of gradient coils are x-gradients, y-gradients, and z-gradients. Suppose a coordinate system is used where  $\mathbf{B}_0$  is parallel to the positive z-direction, and the xy-plane is perpendicular to z. In that case, the gradients and the respective axes can be displayed as in [Figure 12]. The z-axis will parallel the main magnetic field, and the xy-plane will be perpendicular to the main field.



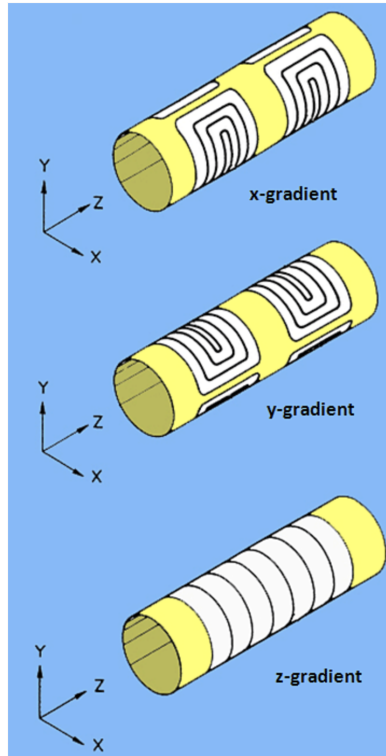


**Figure 12:** Gradient coils. Courtesy of Allen D. Elster, MRIquestions.com[16].

Each set of coils is managed by its own power amplifiers and creates a magnetic field in their respective directions. The x-gradient coils create a magnetic field that varies as a function of x with gradient  $\Delta x$ . The y-gradient coils create a magnetic field that varies as a function of y with gradient  $\Delta y$ . And the z-gradient coils create a magnetic field that runs as a function of z with gradient  $\Delta z$ . The x- and y-gradients do not produce magnetic fields with x- or y-components but rather strengthen or weaken  $B_0$ , depending on the x- and y-coordinates. Most 1.5-3.0T MRI machines operate with a gradient strength of 30-45mT per meter[17]. An image of how the fields vary in strength according to a position is depicted in [Figure 13].

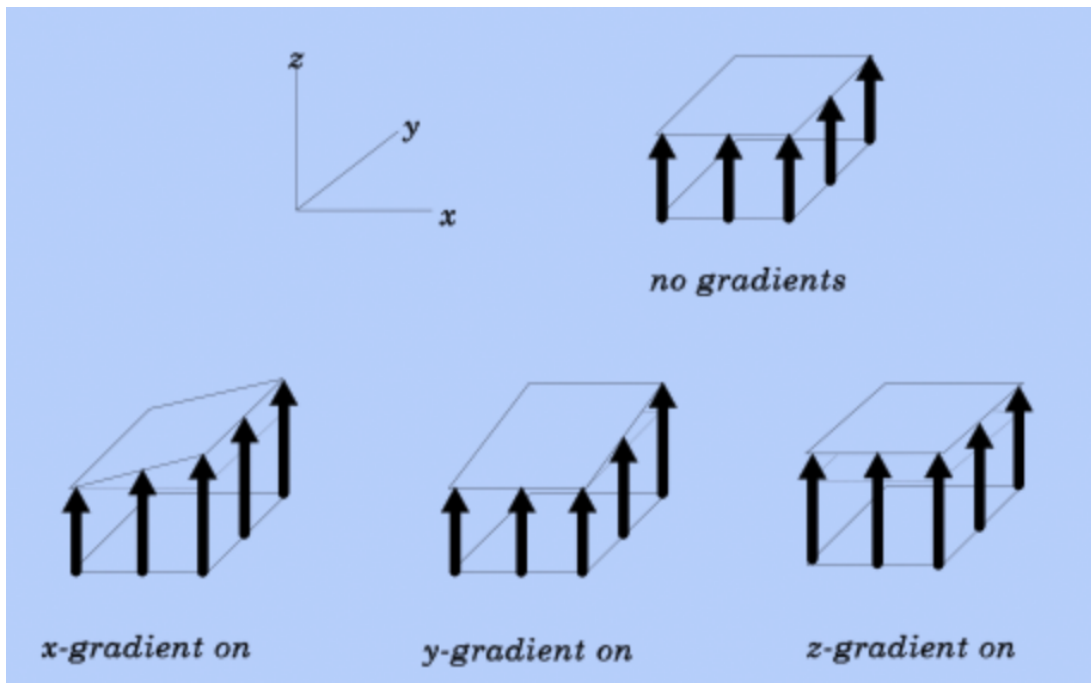


**Figure 13:** Based on a single slice from the whole region inside the cylindrical bore, where the  $z$ -axis is parallel to the main magnetic field, the action of the different gradients is visualized. As this is essentially in two dimensions ( $x$  and  $y$ ), the image shows how the field strength is varied as a function of  $x$  when the  $x$ -gradient is turned on and how it goes as a function of  $y$  when the  $y$ -gradient is turned on. The  $z$ -gradient is homogeneous over the whole region, as this gradient only runs as a function of  $z$ . The combination of the  $x$ - and  $y$ -gradient in the slice give each point a different field strength. Courtesy of Allen D. Elster, MRIquestions.com[16].

### 3 Basics of Magnetic Resonance Imaging

This chapter introduces the mathematical and physical basis of magnetic resonance imaging, basic aspects of image formation, and common MRI contrasts.

#### 3.1 Classical Description

This section provides the equations needed to understand the behavior of nuclear bodies. To establish a small overview; it is the sum of all dipole moments - the collective magnetic moment - from spinning magnetic objects that are the total magnetization and is the signal measured in MRI. Motion, either rotational or linear, has a corresponding momentum - angular or linear momentum. For a proton with velocity  $\mathbf{v}$  and mass  $m$ , this linear momentum  $\mathbf{p}$  is expressed by

$$\mathbf{p} = m\mathbf{v}. \quad (1)$$

Considering an object rotating - *spinning* - with a velocity about a point from a distance  $r$  from this point, the motion is described with an angular momentum vector  $L$ .  $L$  is defined as

$$L = r \times p. \quad (2)$$

Whereas in quantum mechanics, the angular momentum is expressed as

$$L = \frac{Ih}{2\pi} \quad (3)$$

where  $I$  is the spin number ( $\frac{1}{2}$  or  $-\frac{1}{2}$  for the  $^1\text{H}$  isotope) and  $h$  is the Planck's constant.

From equations 1 and 2, it can be derived that the magnitude of the angular momentum can be rewritten as

$$L = mvr \quad (4)$$

with a spinning direction perpendicular to the plane of motion. Furthermore, the angular momentum can be changed when a *torque*  $\tau$  is applied. Torque is defined as the cross product of a force  $F$ , and the distance  $r$  over which the force is applied:

$$\tau = r \times F. \quad (5)$$

With Newton's second law

$$F = \frac{dp}{dt} = ma \quad (6)$$

the torque can be rewritten as such:

$$\tau = r \times F = r \times \frac{dp}{dt} = \frac{dL}{dt}. \quad (7)$$

Thus, the torque is equal to the change in angular momentum.

If a nucleus has an odd number of protons and neutrons added together, it will possess the quantum mechanical property of *spin*. This property cannot be fully explained in classical terms, but the explanations and equations provided are sufficient to understand the spin effect. In the case of hydrogen (the most regarded particle in MRI because of its high abundance in the human body), there is spin, as this nucleus only has a single proton at its core. This means the proton will spin around its own axis and, with its positive charge, behave like a small magnetic dipole. From the right-hand rule, all spinning magnetic objects induce a current loop that generates a magnetic field. This field is characterized by its magnetic moment vector  $\mu$  expressed by:

$$\mu = \frac{ev}{2\pi r} \pi r^2 \quad (8)$$

where  $e$  is the charge of the object and  $v$  is the rotational velocity around a point at a distance  $r$ . Equation [8] shows that the magnetic moment upscales with the object's charge, rotational velocity and the object's distance or radius from the point it rotates about. Furthermore, by using equation [4], a relation connecting  $\mu$  and  $L$  can be obtained:

$$\mu = \frac{e}{2m} L = \gamma L \quad (9)$$

$\gamma$  is the (classical) gyromagnetic ratio and describes the magnetic moment and the angular momentum ratio. This formula for  $\mu$  is also valid for any orbital, periodic motion, including the microscopic motion of elementary particles like hydrogen. A visualization of a proton's magnetic moment  $\mu_p$  can be seen in [Figure 14] below:

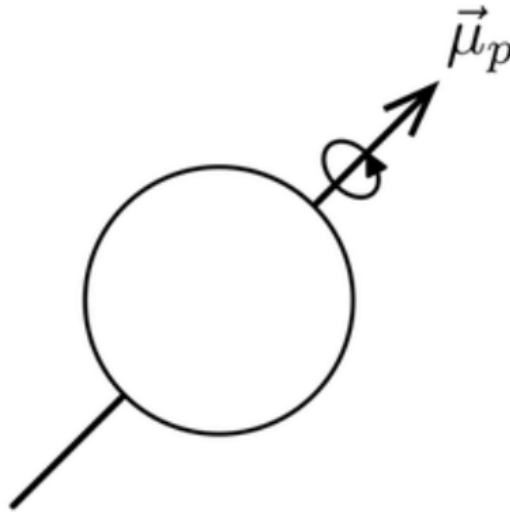


**Figure 14:** A proton spinning about its own axis, inducing a current around its body that consequently generates a magnetic field in the direction of the magnetic moment. Credit for the image goes to David Adair, via <https://www.researchgate.net>[18].

From the equations above, it can be derived that when a hydrogen is situated in a magnetic field  $B_0$ , the loop will experience a torque  $\tau$  expressed by:

$$\tau = \mu \times B_0. \quad (10)$$

Combination of equations [7], [9] and [10] gives:

$$\frac{d\mu}{dt} = \gamma \mu \times B_0. \quad (11)$$

As  $\gamma$  is always constant, equation [11] expresses the fact that  $\mu$  rotates its orientation relative to the  $B_0$  field. Alternatively, the change of  $\mu$  around  $B_0$  can also be described as

$$\frac{d\mu}{dt} = \mu \times \omega. \quad (12)$$

Combining equations [11] and [12] gives:

$$\omega = \gamma B_0 [13]. \quad (13)$$

### 3.2 Nuclei Behavior in a Magnetic Field

In MRI, the techniques involve large collections of protons and their spins. When looking at a sample of  $1\mu\text{L}$  voxel, there are approximately  $6 \times 10^{19}$  proton spins that mostly come from water molecules [5]. Outside of an external magnetic field, the protons' orientations are random, as seen in [Figure 15]:

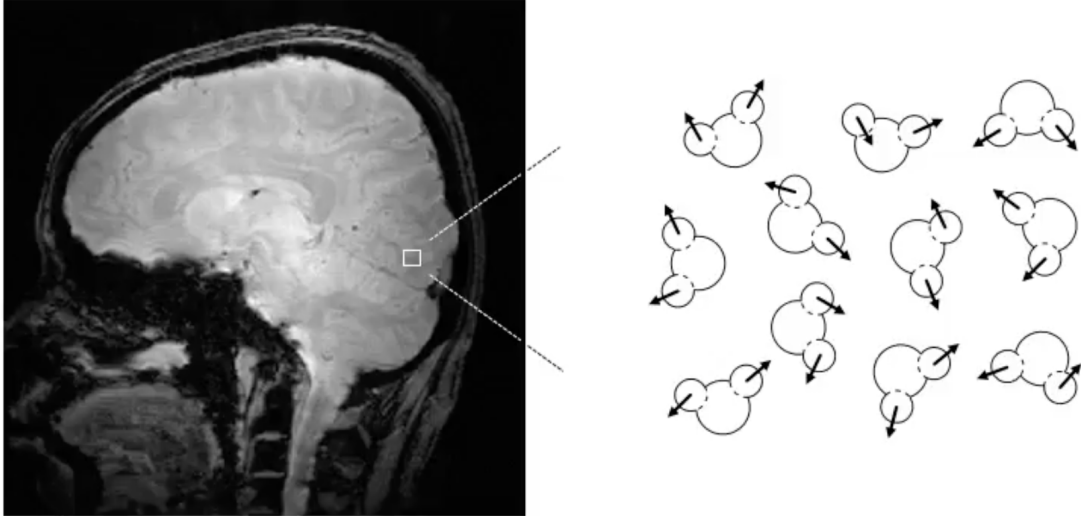


**Figure 15:** Water molecules with two hydrogen each show the random orientations of the magnetic moments when no magnetic field is applied. If anything, the direction of the magnetic moments are decided by the collision between the nuclei. Reprinted by permission from John Wiley And Sons: John Wiley And Sons, Wiley Books. *Basic Principles*, Robin A. de Graaf., 2018[5].

Equation [11] conveys that when protons are exposed to an external magnetic field  $B_0$ , their magnetic moment will orient itself relative to  $B_0$ . For a proton and its properties, this orientation is either parallel or anti-parallel with the field. This builds on equation [13], the Larmor equation. It was derived in 1897 by the late Irish mathematician, and physicist Joseph Larmor[19]. It explains the motion and rate of *precession*, which is the motion of change of direction of the axis of rotation. It is often associated with a spinning top where the axis does not stay vertical. The top slightly wobbles because of a torque acting on it due to gravity.

For protons, precession is the motion of the magnetic moment when placed in a magnetic field. The path of motion is around the direction of  $B_0$  as seen in [Figure 16]. The Larmor equation implies that the stronger  $B_0$ , the higher the precession frequency. With a proton's fixed value of  $\gamma = 2.68 \times 10^8 T^{-1} sec^{-1}$ , the Larmor precession is 42.58MHz per one Tesla field strength.

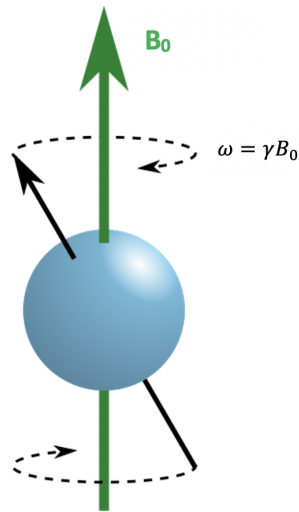


**Figure 16:** A proton precessing about the direction of  $B_0$  (green arrow) with its magnetic moment changing according to the black dotted line. The frequency of precession is  $\omega$ . *Precession in a magnetic field* by FbrG is licensed under CC BY 2.0[20].

Exposing the protons from [Figure 15] to an external magnetic field  $B_0$ , the alignment of the protons' orientations is visualized:

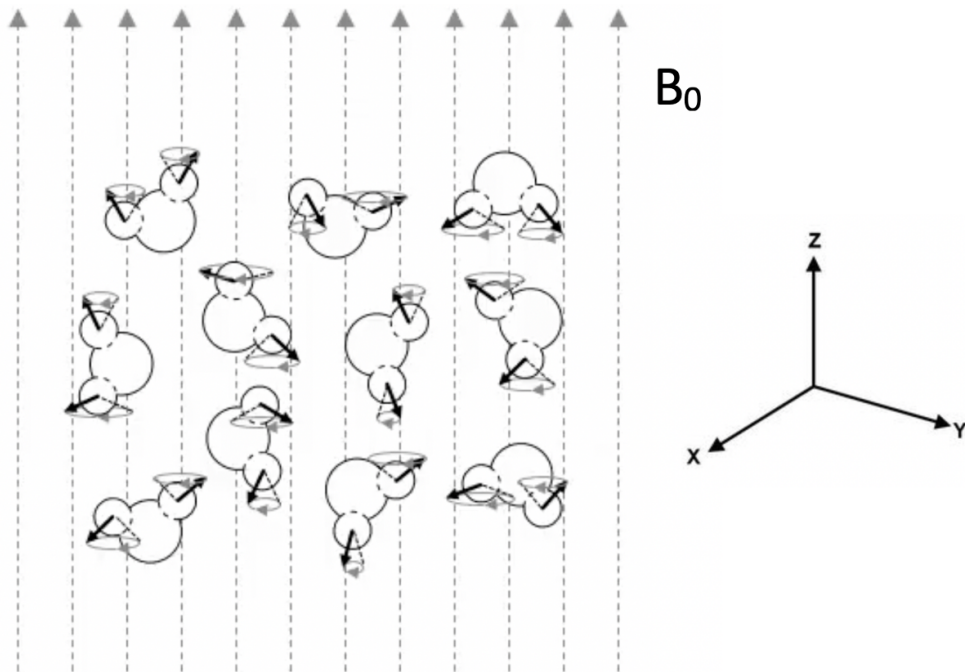


**Figure 17:** A magnetic field  $\vec{B}_0$  is applied to the water molecules. The protons and their spins line up parallel or anti-parallel with  $\vec{B}_0$ . The angle  $\alpha$  at which they precess, is random for every proton. Illustration is adapted, Reprinted by permission from John Wiley And Sons: John Wiley And Sons, Wiley Books. *Basic Principles*, Robin A. de Graaf., 2018[5].

### 3.3 Magnetization

The sum of all magnetic moment vectors per volume element is defined as the *magnetization*. It is a measure of magnet moment intensity and is the actual signal in MRI. In other words, the signal is a function of the number of hydrogen in the sample. When summing two or more vectors, the result is one single vector (the magnetization). By adding vectors of the same magnitude, but in opposite directions, they cancel out, leaving a *net magnetization* of zero. These vector rules define the basis of calculating magnetization.

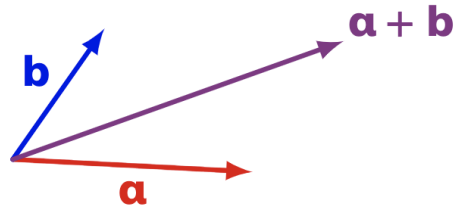


**Figure 18:** The sum of vector  $a$  and  $b$  equals a new vector  $a + b$ . Here no components are pointing in opposite directions. Therefore, the sum vector is bigger than both  $a$  and  $b$ . If  $b$  was anti-parallel to  $a$  with the same magnitude, then they would cancel each other out, and  $a + b$  would be zero.

For  $>99.9\%$  of protons in a voxel under the influence of a field  $B_0$ , a proton will be pointing in the exact opposite direction. This leaves a net magnetization of zero among these  $>99.9\%$ . However,  $<0.1\%$  will adopt a "spin-up" state with no proton in the opposite. This results in a net magnetization in the direction of the  $<0.1\%$ . If  $B_0$  points in the  $+z$ -direction, the net magnetization  $M_0$  can be expressed as the sum of all protons' magnetic moments:

$$M_0 = (N_1 - N_2)\mu \quad (14)$$

where  $N_1$  and  $N_2$  are the amount of protons parallel and anti-parallel with the field, respectively. This is called the *longitudinal magnetization* and is a state of thermal equilibrium. To visualize how the collection of protons is distributed in a voxel in an applied magnetic field, all magnetic moments are put on the origin of the same 3D grid.  $>99.9\%$  of protons is split from the  $<0.1\%$  in the "spin-up" state as illustrated in [Figure 19] below.

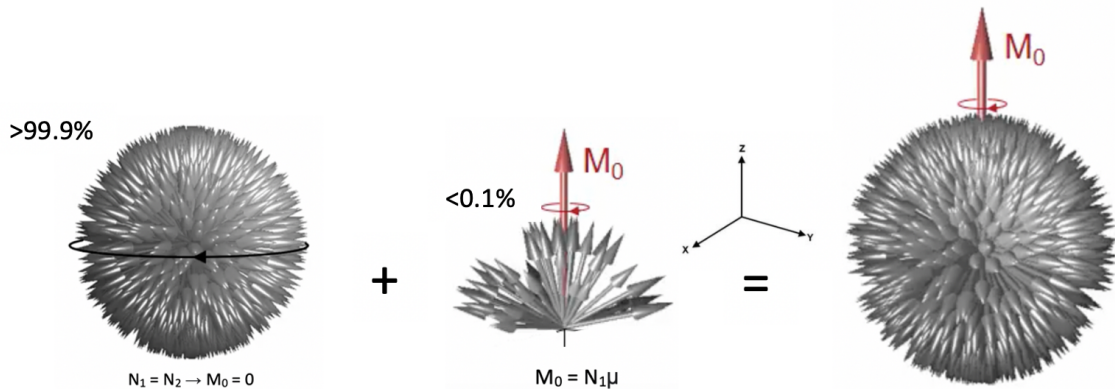


**Figure 19:** Looking like a sphere made of spikes, one spike is one magnetic moment vector. Adding together  $>99.9\%$  of the magnetic moments yield zero magnetization. The remaining  $<0.1\%$  will account for the total magnetization in the voxel. Illustration is adapted, Reprinted by permission from John Wiley And Sons: John Wiley And Sons, Wiley Books. *Basic Principles*, Robin A. de Graaf., 2018[5].

At thermal equilibrium, the signal from the longitudinal magnetization is undetectable as it is inferred by the much stronger  $B_0$ . If the total magnetization is defined as  $\vec{M} = [M_x, M_y, M_z]$  then  $\vec{M} = [0, 0, M_0]$  at equilibrium.

### 3.4 Excitation

To measure  $M_0$ , it has to be separated from  $B_0$ . What distinct  $M_0$  from  $B_0$  is the Larmor frequency. The protons can transition between different energy states if the appropriate energy is absorbed. The energy difference  $\Delta E$  between equilibrium and the so-called high energy state is:

$$\Delta E = \gamma |B_0| \hbar \quad (15)$$

where  $\hbar = \frac{h}{2\pi}$  is the reduced Planck's constant.

In order to read the signals from  $M_0$ ,  $B_1$ , a secondary magnetic field (often regarded as a "pulse") is introduced. This is the field induced by the RF coils, as explained in chapter 2.3. If the frequency of the sinusoidal waves from  $B_1$  equals the Larmor frequency of the protons, the energy from  $B_1$  will be absorbed. From energy absorption, the protons will start synchronizing their spins. There will be a "phase coherency" where all the protons spin at Larmor frequency. The  $B_1$  pulse is usually perpendicular to  $B_0$  (a  $90^\circ$  pulse); the pulse will flip the proton spins away from the z-axis and onto the transverse plane in an act called *excitation*. Thus, the  $<0.1\%$  protons will go from inducing a net magnetization on the z-axis to rotating on the xy-plane as seen in [Figure 20]. When  $M_0$  is induced perpendicular to the z-axis, the magnetization can be detected as it's no longer inferred by  $B_0$ .

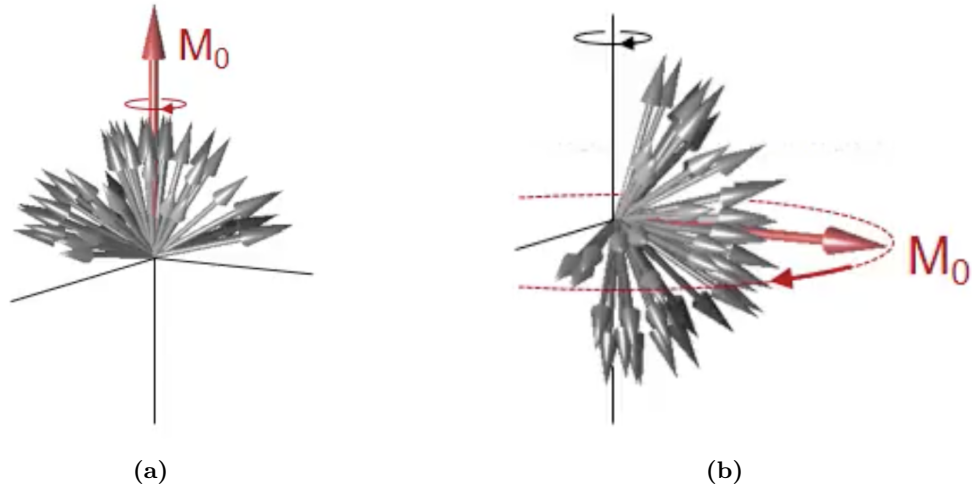


**Figure 20:** (a) The  $<0.1\%$  of protons inducing a magnetization in the z-direction.  $M_0$  is undetectable as the much stronger field  $B_0$  points in the same direction. (b) A  $90^\circ$  pulse is sent into the tissue at the correct frequency, and absorbed by the precessing protons. This flips the spins leading to a rotation on the xy-plane. Illustration is adapted, Reprinted by permission from John Wiley And Sons: John Wiley And Sons, Wiley Books. *Basic Principles*, Robin A. de Graaf., 2018[5].

The synchronized spinning rhythm, the phase coherency, is the *resonance* part of MRI. The resonance is what induces the magnetization, which can be referred to as the *transverse magnetization*  $M_0^{xy}$ . As  $M_0$  was solely on the z-axis, the magnetization will now be split between the x- and y-axis giving two non-zero parameters for  $\vec{M}$ . The net magnetization vector can now be expressed by,

$$\vec{M} = [M_0^x, M_0^y, 0]. \quad (16)$$

The process of turning on and off the  $B_1$  field and detecting the change in longitudinal and transverse magnetization lays the foundation for the technique behind acquiring an image in MR.



### 3.5 T2 Relaxation

As the protons are resonating,  $B_1$  is shut off. The local environments in the tissues make it so each proton rotates at a slightly different frequency. These local anomalies include inhomogeneity in the external magnetic field, and collisions of protons. Tissues with a proton-dense environment, will therefore have a shorter relaxation time than less proton-dense tissues. These factors lead to a de-synchronization of the resonating spins within milliseconds. The loss of phase coherency forces a decay of the transverse magnetization without energy loss. The time it takes for 63% of the protons to dephase and "relax" is called  $T_2$ . The process of phase de-synchronization is called  $T_2$  relaxation, or "spin-spin" relaxation. A general rule regarding loss of magnetization is that after 5 times  $T_2$ , all the magnetization has been lost. [Figure 21] visualizes the spin-spin relaxation for protons in a tissue with a  $T_2$  of 200ms.

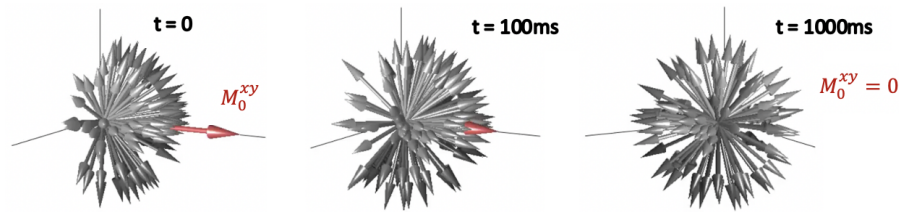


**Figure 21:** The left image shows the protons' magnetization just after excitation. They rotate in resonance, inducing the maximum transverse magnetization. After 200ms, 63% of the protons have phase-shifted due to some rotating faster and slower than others. This de-synchronization leads to vector components canceling each other out, which lessens the transverse magnetization to 37% of maximum. Still rotating on the transverse plane, after 1000ms (5 times  $T_2$ ), all protons have dephased and canceled each other out. Thus, the net magnetization after adding all magnetic moment vectors is zero. Illustration is adapted, Reprinted by permission from John Wiley And Sons: John Wiley And Sons, Wiley Books. *Basic Principles*, Robin A. de Graaf., 2018[5].

The loss of transverse magnetization follows the equation

$$M_{xy}(t) = e^{-t/T_2} \quad (17)$$

which is the *free induction decay* (FID) curve as seen in [Figure 22] below.

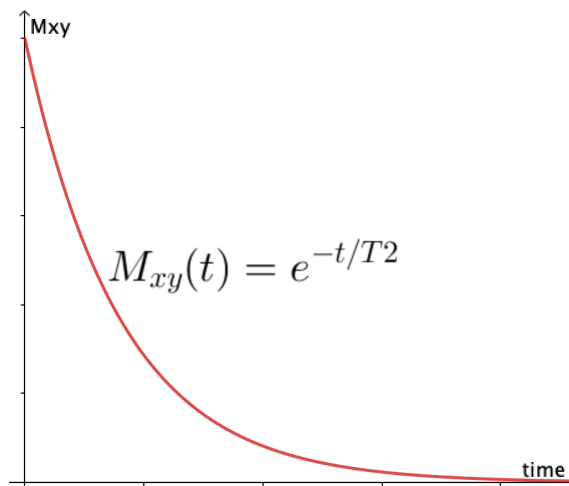


**Figure 22:** The free induction decay plot, showing the loss of transverse magnetization as a function of time.

The time  $t$  is the time passed from when  $B_1$  is shut off, to when the signal is detected by the receiver coils. This is also known as the *echo time*, because it resembles an echo when transmitting signals into the tissue, and receiving signals back.

### 3.6 T1 Relaxation

Excited atoms do not hold on to the energy for long. In the range of 0.1 to 4.0 seconds, depending on the tissue, the protons "relax" their spins back to equilibrium in a process called *T1 relaxation*. The net energy from the excited state is emitted back into the tissue.  $M_0$  is restored in the longitudinal direction. As such, the change in the total magnetization  $\vec{M}$  goes from  $\vec{M} = [M_0^x, M_0^y, 0]$  in the excited state, to  $\vec{M} = [0, 0, M_0]$ .

Picking up from the rightmost image in [Figure 21], the restoration of  $M_0$  in the z-direction is visualized in [Figure 23].

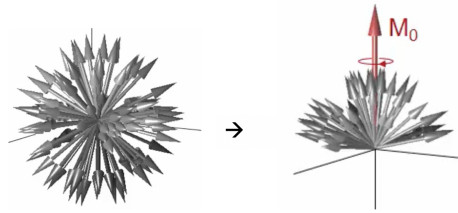


**Figure 23:** The net magnetization equals zero in all directions after T2 relaxation. However, it grows in the z-direction as the protons emit energy into surrounding tissue and flip their spins back to equilibrium. Therefore, the net total magnetization will never be zero. Note that the longitudinal magnetization will have started regrowing before the complete loss of transverse magnetization in practice. Illustration is adapted, Reprinted by permission from John Wiley And Sons: John Wiley And Sons, Wiley Books. *Basic Principles*, Robin A. de Graaf., 2018[5].

T1 relaxation follows the same principle as T2 relaxation in that different tissue exhibit different T1 values. The equation [16] expresses the restoration of magnetization in the z-direction.

$$M_z(t) = 1 - e^{-t/T1} \quad (18)$$

where  $t$  is the total time after excitation. Therefore, T1 will always be equal to, or bigger than T2. Similar to T2 relaxation, the complete restoration of the longitudinal magnetization is seen after 5 times T1.

The relaxation of proton spins after excitation follows the curve of an upside-down conical helix. The FID plot is combined with the equation for T1 relaxation to produce a 3D plot of the change in the total magnetization as seen in [Figure 24].

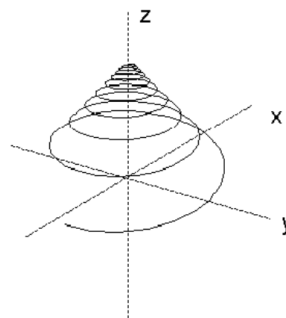


**Figure 24:** The trajectory of  $\vec{M}$  relaxing back to equilibrium. Credit goes to Behrooz Fateh[21].

### 3.7 Image Acquisition

MRI sequences generate signals from entire tissue inside the scanner within the transmit and receive RF coils. Without a predefined spatial localization, the obtained MR signal will represent the whole body. To acquire spatial information from the tissue, we should find a way to separate signals from different body regions.

To produce an image with MR, precession frequency, proton density, magnetism, excitation and relaxation is all put together. When imaging, the signals emitted by the resonating protons arise from multiple voxels simultaneously, which then has spatially encoded by *spatial encoding*. Spatial encoding involves purposely distorting the external magnet field with the use of the gradients. The signals that are received back (the echo) is thus the sum of many free induction decays and echoes from voxels that have unique frequencies, phases and amplitudes. There are three main steps in localization of the signal.

#### 3.7.1 Slice Selection

Localization is greatly done by using magnetic gradients. While the main field  $B_0$  cannot change, additional weaker magnetic fields can be locally disturbed by changing and controlling electrical currents through dedicated coils, the gradients located on the inner side of the magnet.

The first step to localization is slice selection. Slice selection is changing the magnetic field strength throughout the external magnetic field as a function of z-coordinates. This is done by applying a *gradient* to the field with the help of the z-gradient. The protons' frequencies will also vary by having a magnetic field with different field strengths throughout. Then, a *frequency bandwidth* is chosen. This is a range of frequencies that a set of protons will have. The span of the bandwidth decides the thickness of the slice, where one slice will be one section in the external magnetic field, cut in the z-direction. See [Figure 25].

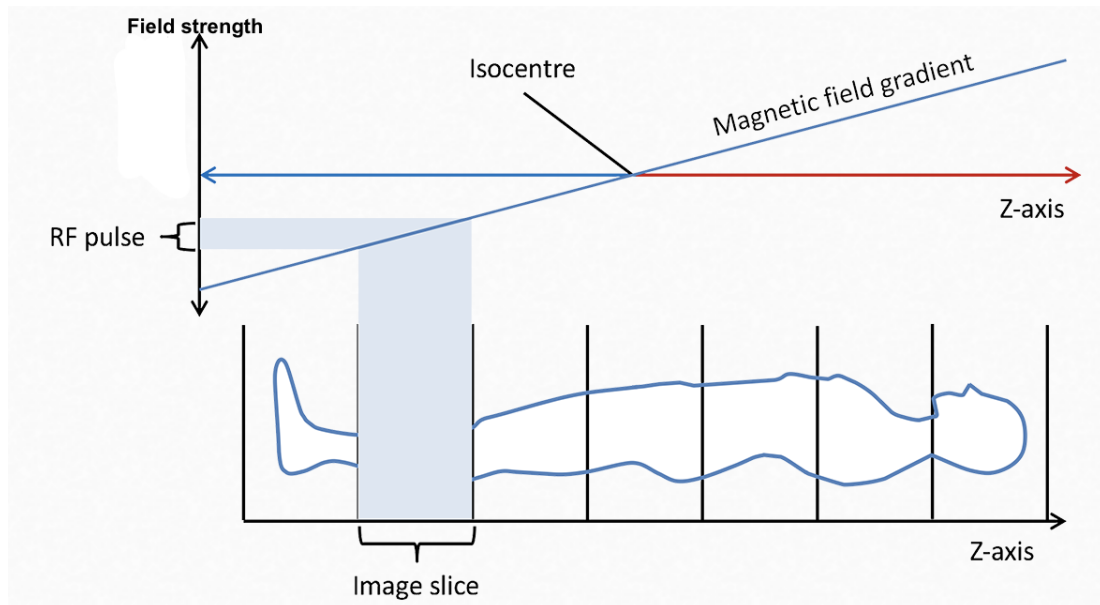


**Figure 25:** The magnetic field strength varies in the z-direction. An image slice with a set field strength range (frequency bandwidth) is chosen. An RF pulse of this frequency is sent into the tissue. The receiver coils are tuned to only detect signals in the frequency bandwidth, and an echo of signals from only this slice is then received. Image credit goes to Radiology Cafe via [www.radiologycafe.com](http://www.radiologycafe.com)[22]. Radiology Cafe retains the intellectual property rights on all material from their website.

In [Figure 26] below is a hypothetical slice of an arbitrary region in the brain.

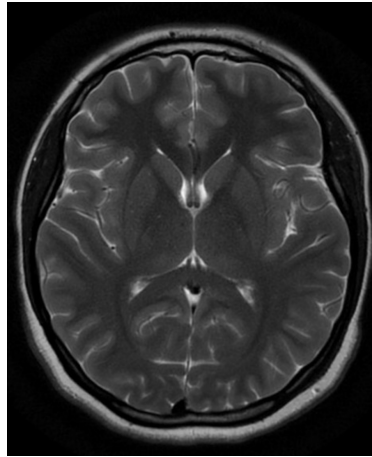


**Figure 26:** An axial slice from the brain. Slices cut in the z-direction (up-down) are considered *axial*. Images "cut" in the x-direction (sideways) are sagittal, whilst coronal images are in the y-direction (front-back). Case courtesy of Dr Gaillard, F. Normal brain (MRI). Case study, Radiopaedia.org[23].

### 3.7.2 Frequency Encoding

After slice selection, the contents of the slice has to be localized. The first step in this process is *frequency encoding*. Frequency encoding enables selection and identification of columns in the slice. In the same way as in slice selection, a frequency-encoding gradient is applied by the x-gradients to change the frequencies of the protons in the slice, column by column. Each column can be localized by tuning the receiver coils to only receive signals from the narrow bandwidth of frequencies of the chosen column. In [Figure 27], [Figure 26] is split into 8 columns, each with a different field strength and frequency.

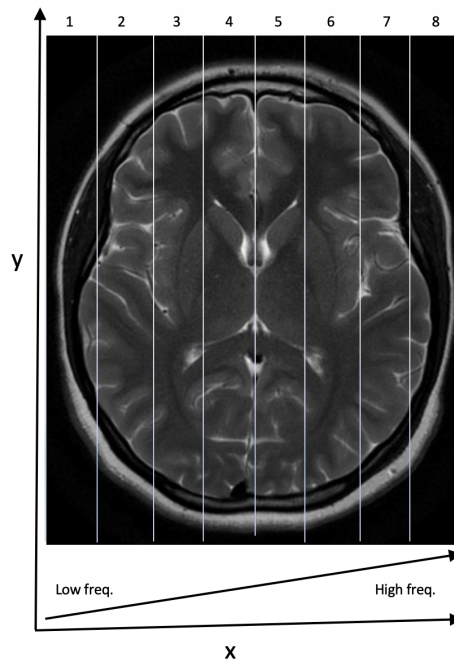


**Figure 27:** The slice from [Figure 26] has been frequency encoded. The frequency increases with  $x$ , enabling localization of each column. Case courtesy of Dr Gaillard, F. Normal brain (MRI). Case study, Radiopaedia.org[23].

### 3.7.3 Phase Encoding

After localization of columns, the slice has localized in the  $y$ -direction. When the  $x$ -gradient is turned off, all protons will precess at the same frequency. However, they will have lost or gained phase relative to the reference state. The signals emitted from voxels in the same column cannot be differentiated. With computer help to do trigonometry and Fourier transforms, each voxel's signal can be detected and differentiated. The calculations done are called phase-encoding steps, which this writing will not go into detail with. If a 2D image has 16 by 16 pixels, there are 256 phase encoding steps. An illustration of the frequency and phase shift is shown in [Figure 28]:

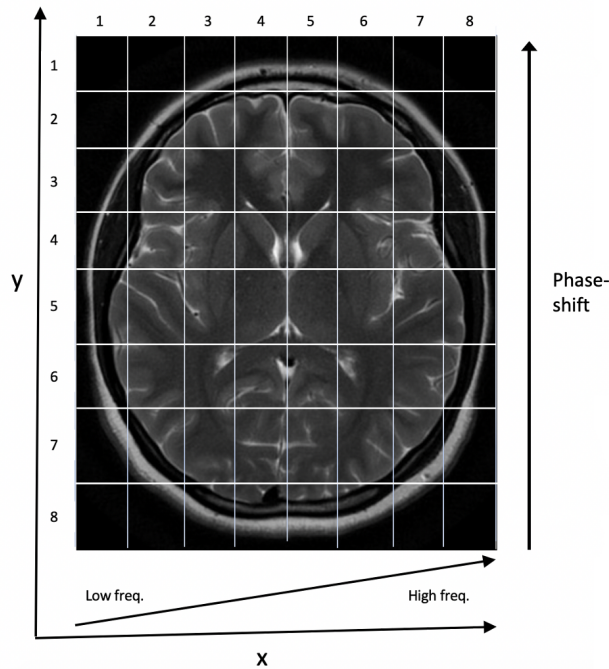


**Figure 28:** Case courtesy of Dr Gaillard, F. Normal brain (MRI). Case study, Radiopaedia.org[23].

Each row in the slice now has a unique phase. A set of systematic Fourier transforms results in each cell being uniquely identified by their signal. Each unique signal/cell is assigned a grey-scale colour, which now technically makes it able to produce a complete image.

### 3.8 Spin Echo and Gradient Echo Sequences

A *spin echo sequence* is the process of re-phasing the protons that de-synchronize following T2 relaxation. This is done by sending a  $180^\circ$  RF pulse in the middle of the echo time (TE) (i.e., TE/2 time after excitation). The  $180^\circ$  pulse will flip the spins 180 degrees, thus reversing the proton spins. The fast-rotating protons will now be "behind" the slowly rotating protons. After an additional TE/2 time, the fast-rotating protons will have caught up with the slowly rotating protons. This results in all protons being in phase at time TE after the initial  $90^\circ$  pulse, thereafter producing a new signal. This particular part of the sequence (i.e., 90 degree-180 degree-acquisition) is repeated every repetition (TR). At each TR, one step of the phase encoding will be recorded ( $G_{phase}$  in [Figure 29]) so that after several TR, all the phase encoding steps will be recorded as visualized in [Figure 29]. The signal from a spin-echo sequence is as follows:

$$S = S_0(1 - e^{-TR/T_1})e^{-TE/T_2} \quad (19)$$

However, the  $180^\circ$  pulse will only "fix" the dephasing caused by proton collisions - not inhomogeneity in  $B_0$ . Therefore, the "echo" signal after the  $180^\circ$  pulse will be slightly weaker than the signal generated right after excitation. The resulting signals can be called the "true T2" signal. As the signal decay is measured purely from the intrinsic properties of the tissue, ruling out the relaxation effects of  $B_0$  inhomogeneity. The true T2 time gives a lot of information about the tissue.

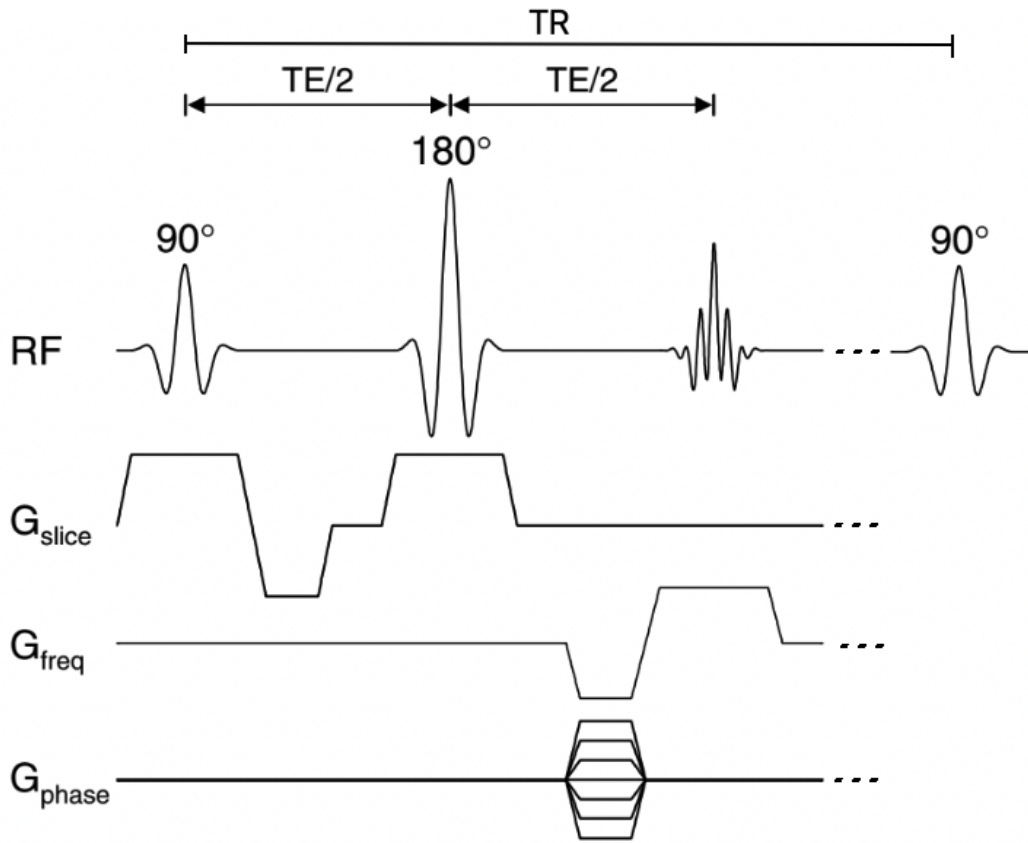


**Figure 29:** Standard spin-echo sequence. The echo time TE is defined from the middle of the 90-degree excitation RF pulse to the middle of the gradient echo, which coincides with the digital-to-analog converter for data sampling. The negative gradient following the pulses are necessary to refocus signal that was dephased during excitation. RF, radiofrequency;  $G_{slice}$ , slice selective gradient;  $G_{freq}$ , frequency encoding gradient;  $G_{phase}$ , phase encoding gradient; TE, echo time; TR, repetition time. Reprinted by permission from John Wiley And Sons: John Wiley And Sons, Wiley Books. *Magnetic Resonance Imaging*, Robin A. de Graaf., 2018[24].

### 3.9 Contrast in MRI

Diverse MR contrasts can be obtained by changing and tailoring the pulse sequence parameters. A pulse sequence consists of several specific elements, such as the strength and duration of excitation and/or refocusing pulses and timing between RF and gradient pulses. Spin density, longitudinal relaxation time T1, and transverse relaxation time T2 are among common parameters to obtain a desired contrast. The scan's repetition time TR and echo time TE are two critical control parameters determining tissue's MR contrast. The TR is the time between consecutive excitation pulses, and the TE determines the duration between excitation pulses and the MR echo.

Repetition time is the period between the applied successive excitation RF pulses. A long repetition time allows the protons in the tissue to relax back to steady-state fully or into alignment with the main magnetic field. A short repetition time will result in the protons from some tissues not having fully rested before the subsequent measurement. This means that the subsequent measurement will not excite full-intensity relaxed protons. Therefore, the generated MR signal or echoes will decrease intensity from the same tissue.

Echo time is the time between the point of the excitation pulse and the peak of the echo signals

received by the coil. Longer echo time will decrease signal intensity in tissues like white matter since the protons are more likely to dephase. Protons in a fluid will remain in phase longer than in denser tissues because the mobility of protons avoids any constraints by physical structures such as axons and neurons. The dephasing effect can be compensated by choosing a shorter echo time.

### 3.10 T1 Weighting

The most common MRI sequences are T1-weighted and T2-weighted examinations. T1 weighted images are produced by determining short TE and TR. The T1 properties of tissues predominately determine the image contrast and brightness. For example, an optimal choice of TE and TR can provide the desired distinction between the white matter and grey matter in the brain by choosing the regions where T1 values of these two tissue types show the more considerable difference [Figure 30].

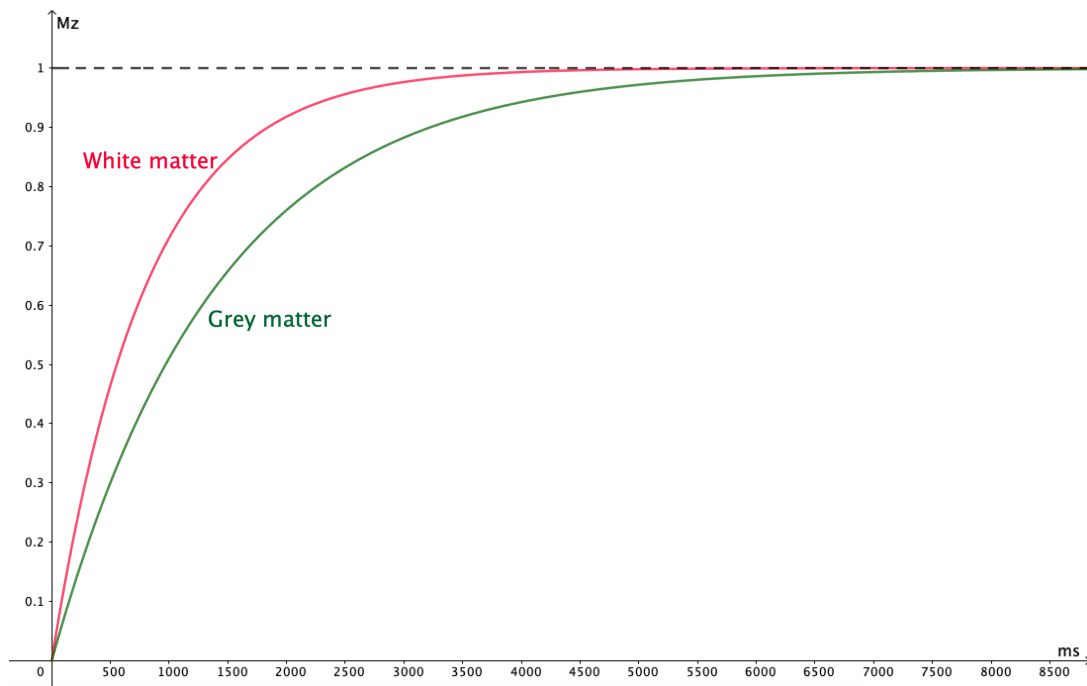


**Figure 30:** The relaxation of longitudinal magnetization in grey matter compared to white matter after excitation.

Longer echo time in the T1 weighted spin-echo sequence of the brain will induce low-intensity images with poorer contrast to noise ratio (CNR). On the hand, the shorter echo time provides an excellent CNR ratio, where the details and margins between white matter and grey matter are obtained. The protons of lipid tissues realign their longitudinal magnetization with  $B_0$  relatively quicker than freely protons of water; therefore, lipid tissues appear brighter on a T1-weighted MR image. Conversely, fluids such as CSF exhibit relatively slower longitudinal magnetization realignment after the excitation. Therefore, CSF has a less transverse magnetization after excitation, leading to lower MR signal and appearing dark.

### 3.11 T2 Weighting

Some tissues and pathological lesions have close T1 properties and values while their T2 properties differ. Thus, a technique to generate contrast with T2 value dependence distinguishes between these types of tissues or lesions. T2-weighted imaging sequence provides such possibilities, providing imaging contrast with proper sequence timing to acquire distinct contrast between tissues with



different T2 properties (e.g., a distinct contrast between grey matter and white matter, see [Figure 31]).

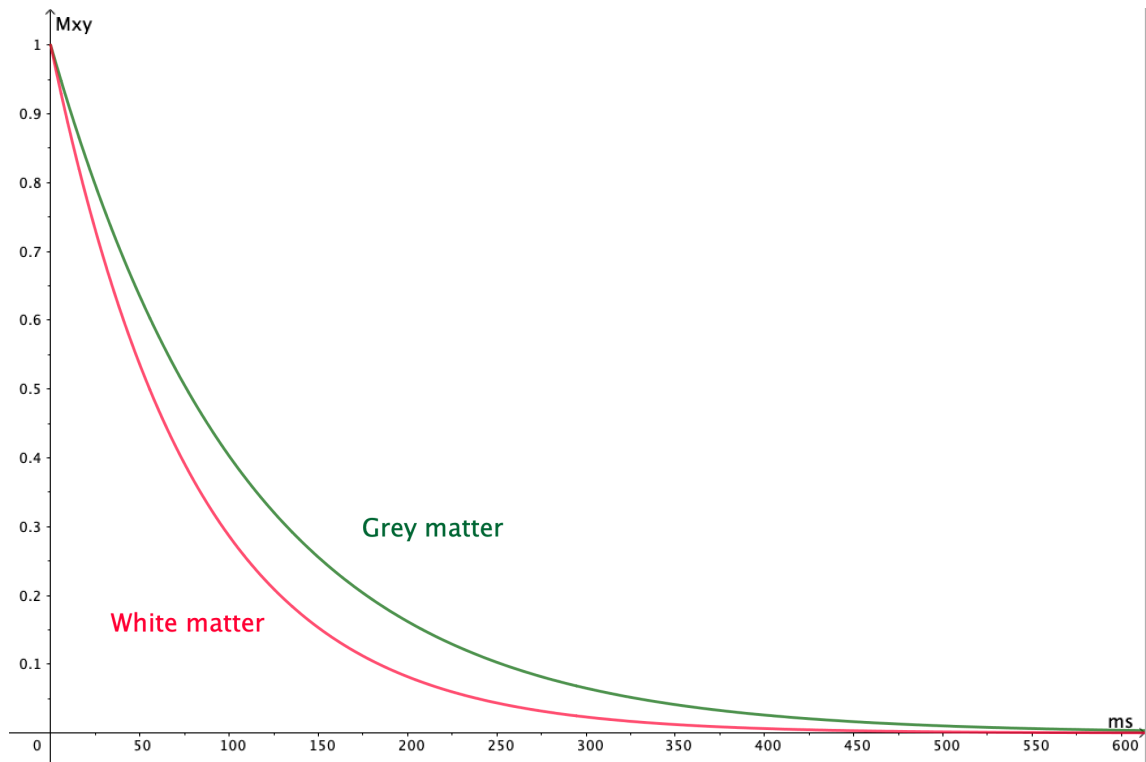


**Figure 31:** The decay of transverse magnetization in grey and white matter. The white matter with a T2 of 80ms, and the grey matter has a T2 of 110ms.

T2-weighting images exhibit brighter intensities in the congregations of neurons of grey matter. The nerve connections of white matter appear gray-ish in the T2-weighted images, while the cerebrospinal fluid appears bright.

## 4 Bloch Simulation

Simulating magnetic resonance is a vital counterpart in the acquisition of MR images. Simulation helps understand the complexity of the MR phenomena and is the most accurate way to study the effect of a pulse sequence on magnetization. It is also extensively used as an educational tool in technical and medical domains[25].

Additionally, simulation can act as a helping tool in developing and optimizing MR sequences. This means it helps find the perfect time between nuclear excitations to produce the best images.

This chapter provides a simulation platform to demonstrate the spin behavior in a strong static magnetic field while reflecting the relaxation parameters. This will be done with computer scripts in Python based on the renowned Bloch equations. The animations are made using FFmpeg, a multimedia framework tool that will decode Python code into GIFs and images. A GIF (a Graphics Interchange Format) is a digital file format that is a short, animated picture or image without sound[26]. GIFs will not be shown in the following sections. However, screenshots will be taken amidst these animations to provide the readers with educational and descriptive demonstrations.

### 4.1 The Bloch Equation

In the same year as the MR phenomena were discovered, Bloch introduced the so-called Bloch equations[3]. These equations are coupled differential equations meant to describe the relaxation and precessional motion of the net macroscopic magnetization from nuclear magnetic moments - all into a single model[4]. Classically, the motion  $\frac{dM}{dt}$  of a single particle obeys the Bloch equation, where the relaxation times and the applied magnetic field strengths are the factors determining how the magnetization changes and develops over time. As the total magnetization is the sum of all dipole moments, the expression for one single particle's magnetic moment is generalized for the total magnetization. Thus, when the tissue sample is placed in a field  $B_0$ , this movement - considered to be a classical vector - is determined by the equation:

$$\frac{dM}{dt} = \gamma \vec{M} \times \vec{B}_0. \quad (20)$$

#### 4.1.1 Frame of Reference

In order to more easily solve the equation, a new coordinate system  $R = (x', y', z' = z)$  is introduced.  $z' = z$  indicates that  $R$  rotates about the z-axis. The rotation speed is denoted  $-\omega$  (which is of the same frequency as the Larmor frequency) and follows the rotation of the  $B_1$  field. The new reference frame  $R$  is known as *the rotating reference frame* and makes finding the magnetization a lot easier, as the field  $B_1$  can be considered as fixed. Considering the original reference frame known as *the laboratory frame* to be  $L = (x, y, z)$ , the two reference frames can be seen in [Figure 32].

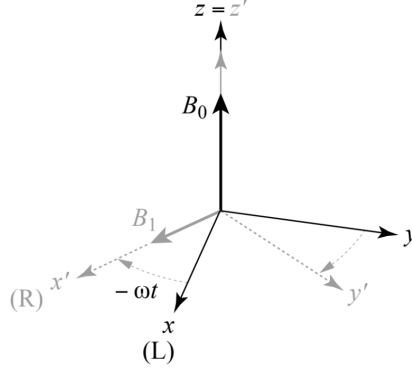


**Figure 32:** The rotating frame of reference  $R = (x', y', z' = z)$  rotating about the z-axis (or  $B_0$  field) at an angular velocity of  $-\omega$ , pictured on top of the laboratory frame of reference. Used with permission of Springer, from *Electron Paramagnetic Resonance Spectroscopy*, Bertrand, Patrick, 2020; permission conveyed through Copyright Clearance Center, Inc.[27].

In the laboratory frame of reference, the change in magnetization when  $B_0$  and  $B_1$  is present is determined as:

$$\left(\frac{dM}{dt}\right)_L = \gamma \vec{M} \times (B_0 + B_1). \quad (21)$$

Whereas in the rotating frame of reference, the same movement is expressed as:

$$\left(\frac{dM}{dt}\right)_R = \left(\frac{dM}{dt}\right)_L - \Omega \times \vec{M}. \quad (22)$$

$\Omega = -\omega$  is the rotation vector of the rotating frame, relative to the laboratory frame. This is used to rewrite the equation for the change in magnetization in  $R$  to:

$$\left(\frac{dM}{dt}\right)_R = \gamma \vec{M} \times B_{\text{effective}} \quad (23)$$

where  $B_{\text{effective}}$  is the "effective field" coming from

$$B_{\text{effective}} = B_0 + B_1 + \frac{\Omega}{\gamma}. \quad (24)$$

## 4.2 Simulations

This section demonstrates simple simulations of spin behavior when protons are placed inside a static magnetic field. The demonstrations include the impact of RF pulses and relaxation in different tissue types including cerebrospinal fluid, lipids, grey matter, and white matter.

At first thought, the following figures and intent will look to be in a similar fashion as the figures displaying relaxation in chapter 3. However, the following simulations will go more in-depth providing specific factors and parameters. Additionally, the figures will be built up by fully customized code to make sure the relevant numbers and content are displayed. Appropriate code such as the values of the tissue-varying parameters used for each simulation are provided.

### 4.2.1 Simulation 1 - 90 degree pulse

MRI sequences and pulse programs are usually started with an excitation pulse with a flip angle (FA) of 90 degree. The 90 degree pulse is emitted from the transmitter part of the RF coils to excite the protons. The pulse angle is perpendicular to the direction of external magnetic field ( $B_0$  along to the z-axis), inducing a strong signals. The receiver coil elements of the RF coil will

later, as predefined in the pulse sequence program, receive MR signals and echos emitted from the protons.

[Figure 33] shows nine protons from water in the rotating frame of reference, where they are excited by a 90 degree pulse. For showcase purposes, the excitation pulse lasts for 1 millisecond. Inside this millisecond, the protons will flip their spins over onto the transverse plane:

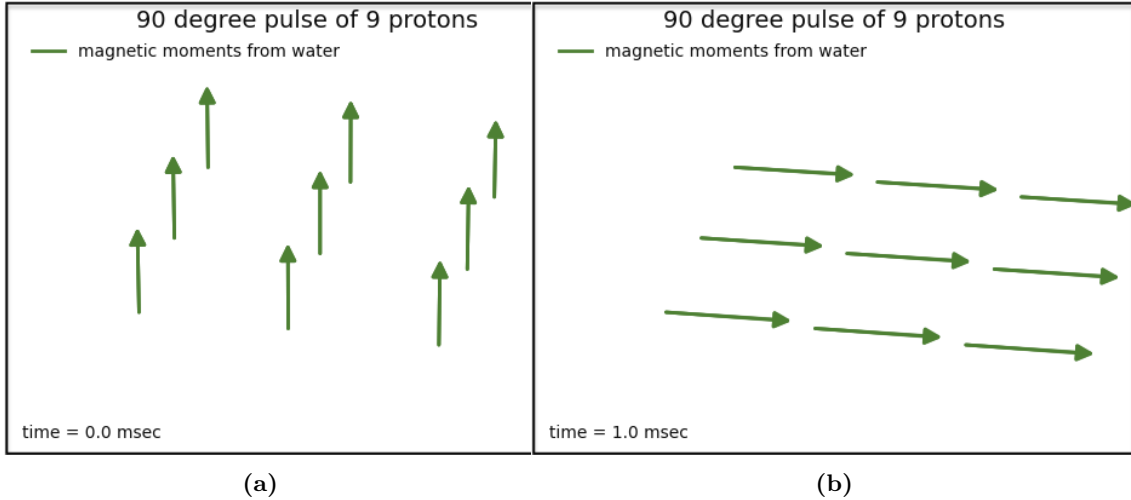


**Figure 33:** (A) Pre-excitation of magnetic moments from 9 protons. The magnetic moments are in equilibrium parallel with  $B_0$  pointing in the +z-direction. The total magnetization is longitudinal. (B): Post-excitation. A 90 degree pulse at the Larmor frequency is sent to excite and flip their spins. As this is from the rotating frame of reference and a homogeneous magnetic field is assumed, the vectors follow an arc path from the z-axis down on the xy-plane where a transverse magnetization is induced.

The parameters in the code used for this simulation is seen below.

---

```
pulseSeq:
-   t: 0
    FA: 90
    dur: 1.0
```

---

A pulse sequence *pulseSeq* is defined to start at time equals zero, with a flip angle of 90 °and lasting for 1.0 ms. For the excitation to be complete after exactly 1ms, the magnitude of the excitation pulse  $B_1$  would have to be  $5.87\mu T$  following the equation for the flip angle  $\alpha$ :

$$\alpha = \gamma B_1 \tau \quad \Rightarrow \quad B_1 = \frac{\alpha}{\gamma \tau}$$

where  $\tau = 1ms$ ,  $\gamma = 42.58 \frac{MHz}{T}$  and  $\alpha = 90^\circ = \frac{\pi}{2}$ .

Recollecting that the net magnetization is denoted  $M_0$ , the excitation leads to a total loss of longitudinal magnetization ( $\vec{M} = [0, 0, M_0]$ ) and regrowth of the magnetization solely on the transverse plane ( $\vec{M} = [M_0^x, M_0^y, 0]$ ). In [Figure 36] the y-axes show reference values with span from 0 to 1. 0 means 0% of  $M_0$ , whilst 1 equals 100% of  $M_0$ .

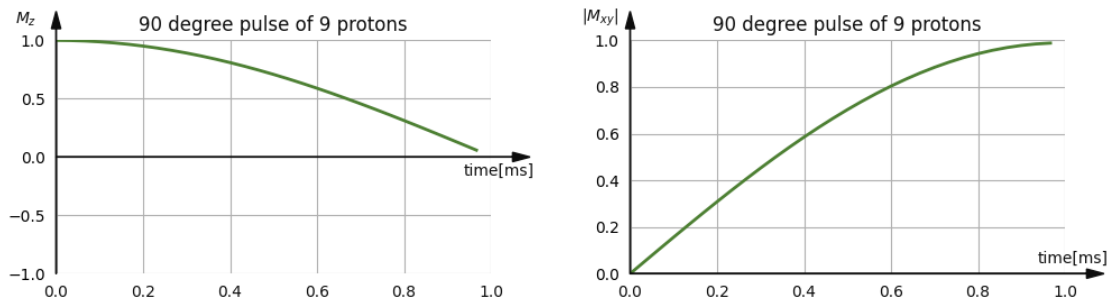


**Figure 34: Figure A:** Following excitation, the decline of the longitudinal magnetization happens. The y-axis spans  $[-1, 1]$  because of the possibility of anti-parallel spins inducing a magnetization in the  $-z$ -direction. **Figure B:** The growth of transverse magnetization as seen following excitation.

#### 4.2.2 Simulation 2 - T2 Relaxation

Shortly after excitation, the transverse magnetization starts to decay. The transverse magnetization is lost faster in proton-dense tissues as more protons push on each other, which speeds and slows down the precession frequency.

This simulation follows a hypothetical T2 relaxation of protons in fat in the brain. The parameters are as follows:

---

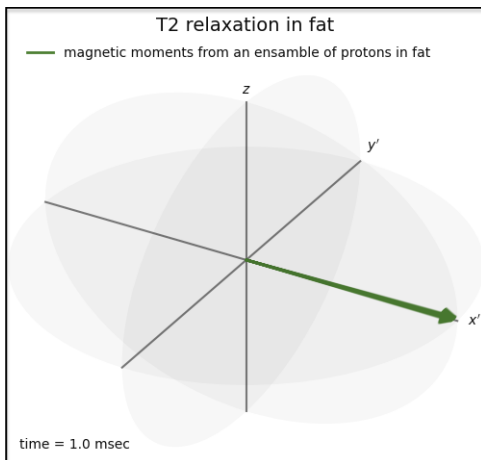
```

B0: 3.0
components:
  - name: fat
    T1: 250.0
    T2: 80.0
nIsochromats: 20

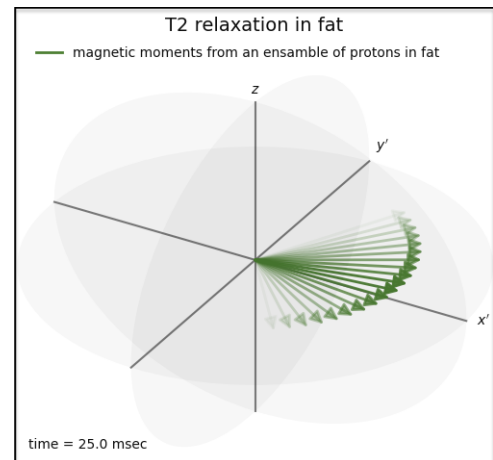
```

---

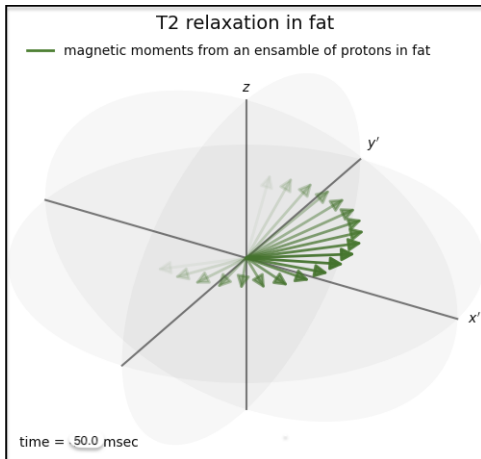
The protons are under the influence of a magnetic field "B0" with a strength of 1.5T, a T1 of 250ms, and a T2 time of 80ms which are the approximate measure of relaxation times for lipids in a 3.0T magnetic field in the brain[28]. "nIsochromats" define the amount of proton isochromats. One isochromat is regarded as an ensemble of protons with the same precession frequency. Hence, the simulation has 20 ensembles of protons, each with a different precession rate. In [Figure 35], 20 proton isochromats from lipid are seen fanning out from the initial position after excitation. This is best visualized in the rotating frame of reference. 19 of the isochromats precess slightly slower or faster than the one isochromat in the middle which appears to not move but only decreases in the x-direction. The magnitude of all isochromats also decreases.



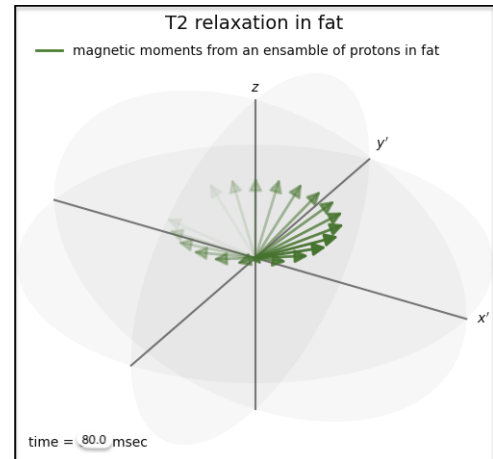
(a) The protons are excited in the same way as in Simulation 1. After a time of 1.0ms, the spins start dephasing.



(b) After 25.0ms the loss of phase coherency looks like the opening of a Chinese fan. The magnitude of the magnetic moments is also seen gradually receding.



(c) The loss of phase coherency is seen after 50.0ms.



(d) After T2 time (80ms), 63% of the protons have dephased. Thus the magnitude in the XY-plane is 37% of the initial value.

**Figure 35:** A display of how protons with a slightly different precession frequency dephase in time. Fats have a short T2 relaxation time compared to water because of more frequent spin-spin interactions pushing protons away from each other and affecting the precession frequency.

The signal from the transverse magnetization is lost following free induction decay, as seen below. The FID plot will not show sinusoidal patterns, only a curved line. [Figure 36] includes T2 relaxation from both fat *and* cerebrospinal fluid (CSF) in the brain. The T2 relaxation time for CSF is set to 1500ms in a 1.5T field following a study done by H.B.W. Larsson[29].

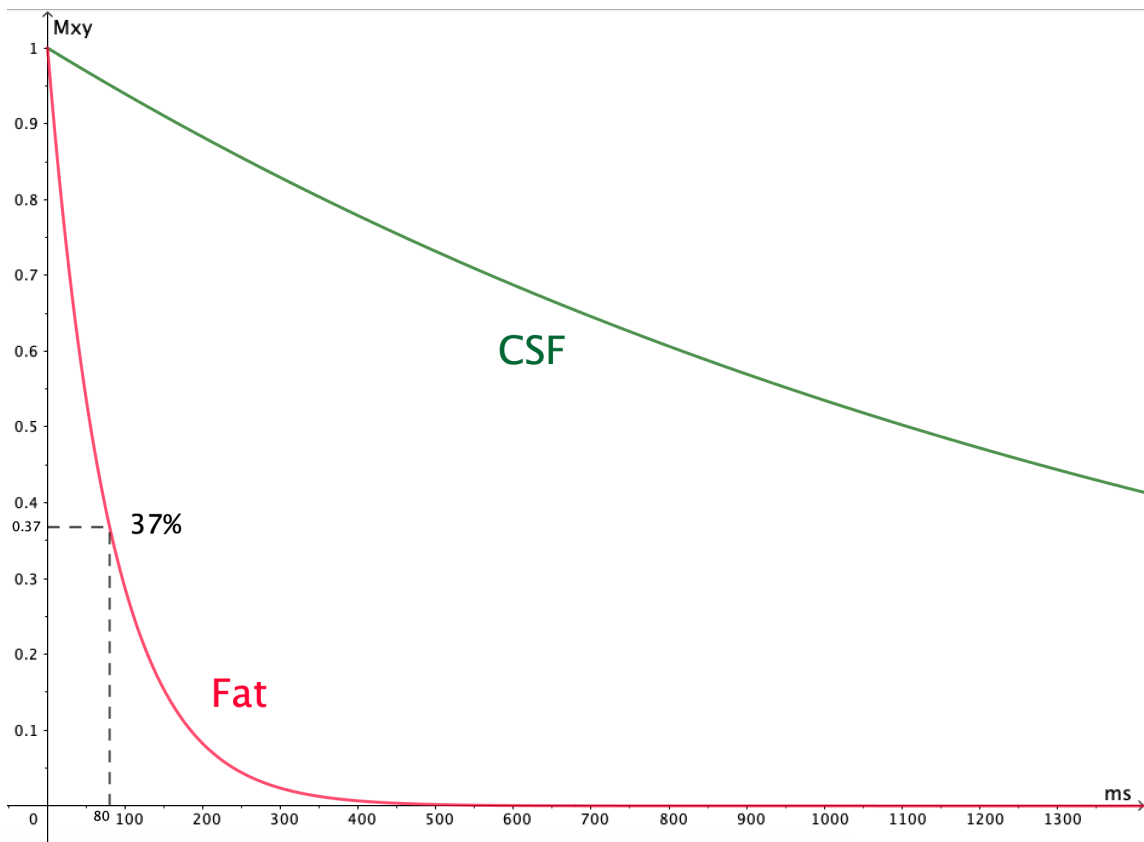


**Figure 36:** The transverse magnetization decays as a function of time. The sine component of the functions is removed to get a clearer display of the decay rate. With the T2 relaxation of 1500ms, the red CSF curve is seen decaying much slower than the green curve from fat, which has a T2 relaxation of 80ms. The graphs follow the equation of  $M_{xy} = e^{-(t/T2)}$ . For fat, this equals about 0.37 after 80ms, as seen in the image. This confirms that 63% of the protons have dephased after T2 time. After approximately 5 times T2, the transverse magnetization is gone in both tissues.

#### 4.2.3 Simulation 3 - T1 Relaxation

Lipid tissue has a relatively small T1 as a result of proton density. Therefore, the strength of the external magnetic field will affect the protons' relaxation time more than it would in, for example, pure water. In a study by Chen Lin in 2001[30], it was found that CSF is not affected by magnetic field strengths. At least not between 1.5 and 4.0T. From the last simulation, the number of isochromats is reduced to one single proton as spin-spin relaxation is not focused. The parameters are set to:

---

```

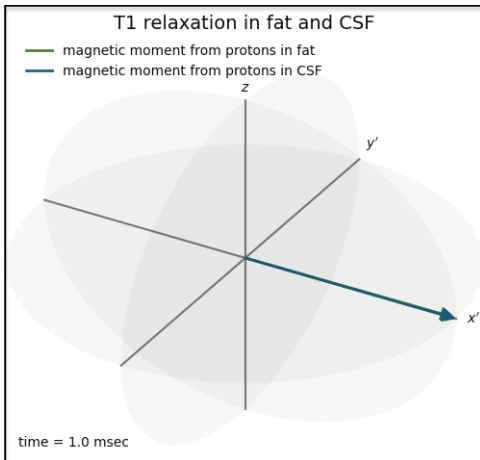
B0: 1.5
components:
  - name: fat
    T1: 250.0
    T2: 80.0
  - name: CSF
    T1: 4200.0
    T2: 1500.0

```

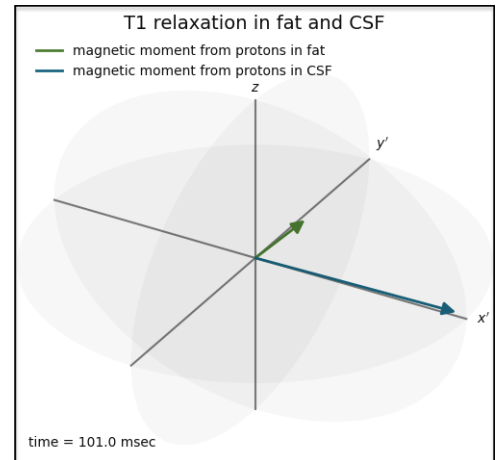
---

where "nIsochromats" is no longer defined, giving a default value of 1. The T1 relaxation of CSF is set to be 4200ms following[30].

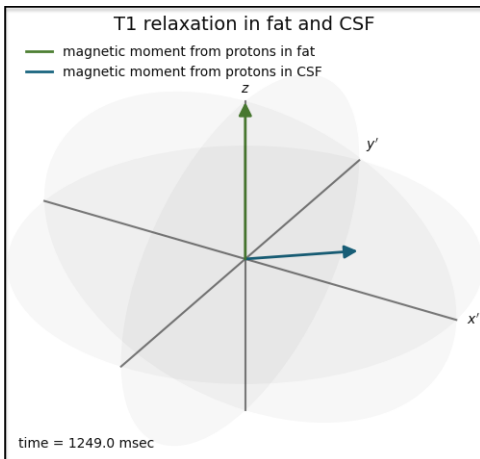
Still, in the rotating frame of reference, a  $90^\circ$  pulse is transmitted and absorbed by the protons in fat and CSF. Shortly after, the longitudinal magnetization starts growing. With the current simulation script, it was not possible to draw a z-component from the vectors in [Figure 37]. However, the growth of the longitudinal magnetizations can still be seen if looking at the vector's z-components in the different time frames.



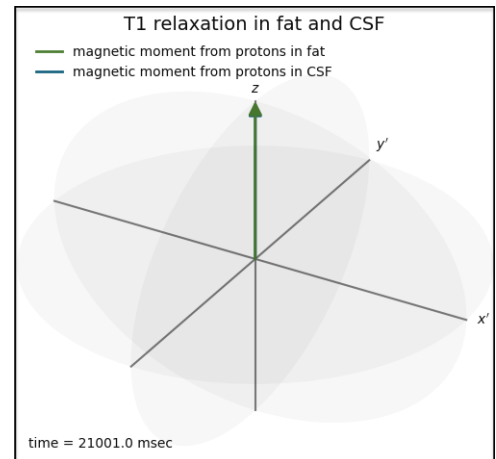
(a) The initial position of the magnetic moments after excitation before the relaxation starts. Here, the longitudinal magnetization in both tissues is zero.



(b) As seen in the image, the fat (the green vector) quickly gains magnetization in the longitudinal direction. As T1 in fat is 250ms, the z-component of the magnetization after 101ms is at  $1 - e^{-0.101/0.25} = 33\%$  of its maximum value. With its much longer T1, the longitudinal magnetization of CSF won't have recovered much. The blue vector displays this.



(c) After 5 times T1 of fat (1250ms), the protons in the lipid tissue will have fully recovered to equilibrium. By this time, the longitudinal magnetization in CSF will have recovered to  $1 - e^{-1.25/4.2} = 26\%$  of its maximum value.



(d) Both tissues have no fully recovered to equilibrium post-excitation, after 5 times T1 of CSF (21 seconds).

**Figure 37:** From excitation to total alignment with the external magnetic field - the process of T1 relaxation in fat and CSF. The differences in relaxation times are easily seen in these four images.

In [Figure 38], the regrowing of longitudinal magnetization is plotted for both tissues. They both



follow the same equation but with different T2 parameters.

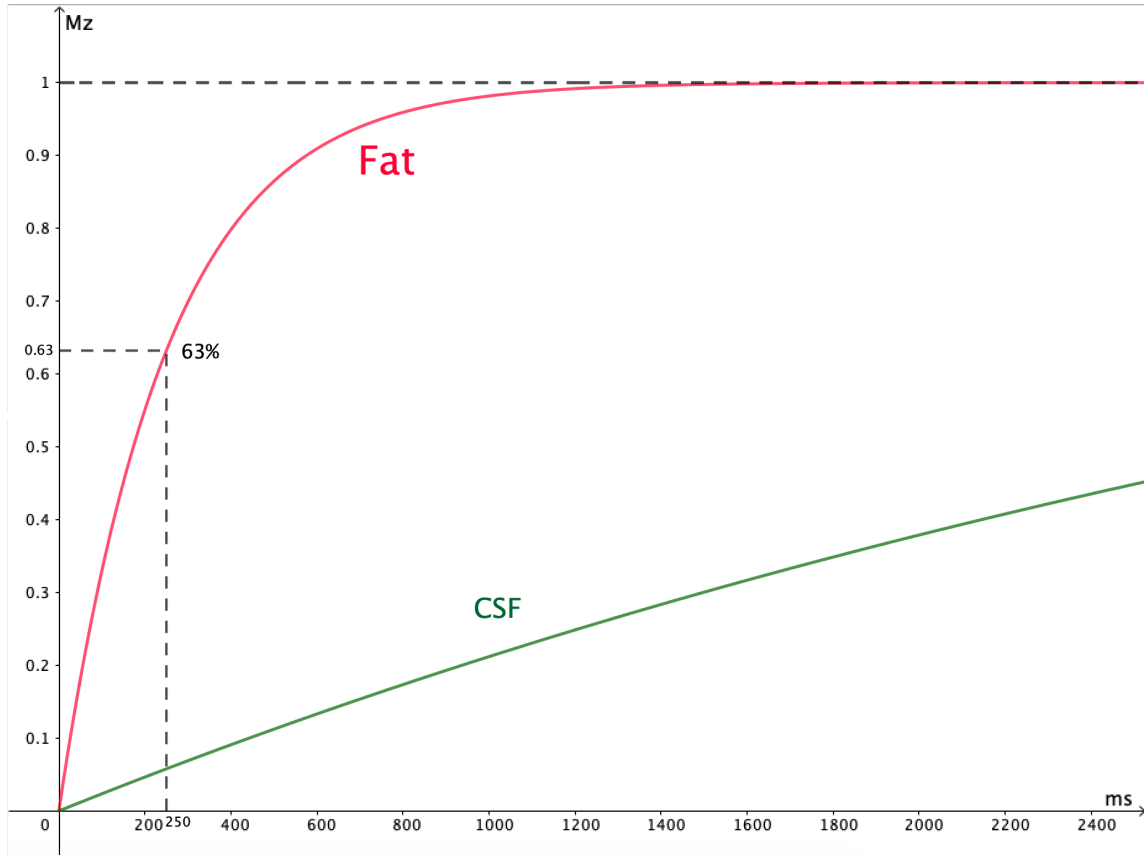


**Figure 38:** The restoration of 63% of the longitudinal magnetization in fat is pointed out after 250ms. After approximately 1250ms, the fat will have fully regrown to its equilibrium. CSF has a much longer relaxation time and therefore spans out of the scope of this plot, but it follows the same curve. Both tissues follow the same equation for the curve;  $M_z = 1 - e^{-t/T2}$ .

#### 4.2.4 Simulation 4 - T1 and T2 Relaxation in grey and white matter

Grey matter is tissue in the brain that homes neural cell bodies, dendrites, axon terminals, and nerve synapses. These structures process signals from the sensory organs and simulates neurons in the CNS (central nervous system), which then induce a response to these stimuli. White matter is bundles of axons coated with proteins and lipids (myelin). This tissue is responsible for communication between the grey matter and the rest of the body by conducting, processing, and sending nerve signals through the spinal cord. These two issues make up the grey and white parts of an MR image.

In the 2001 study by Chen Lin[30], it was found that in a 3.0T field, the grey matter had a T1 relaxation time of about 1400ms, while the T1 of white matter was around 800ms. The two tissues' T1 relaxation is compared in [Figure 39]:

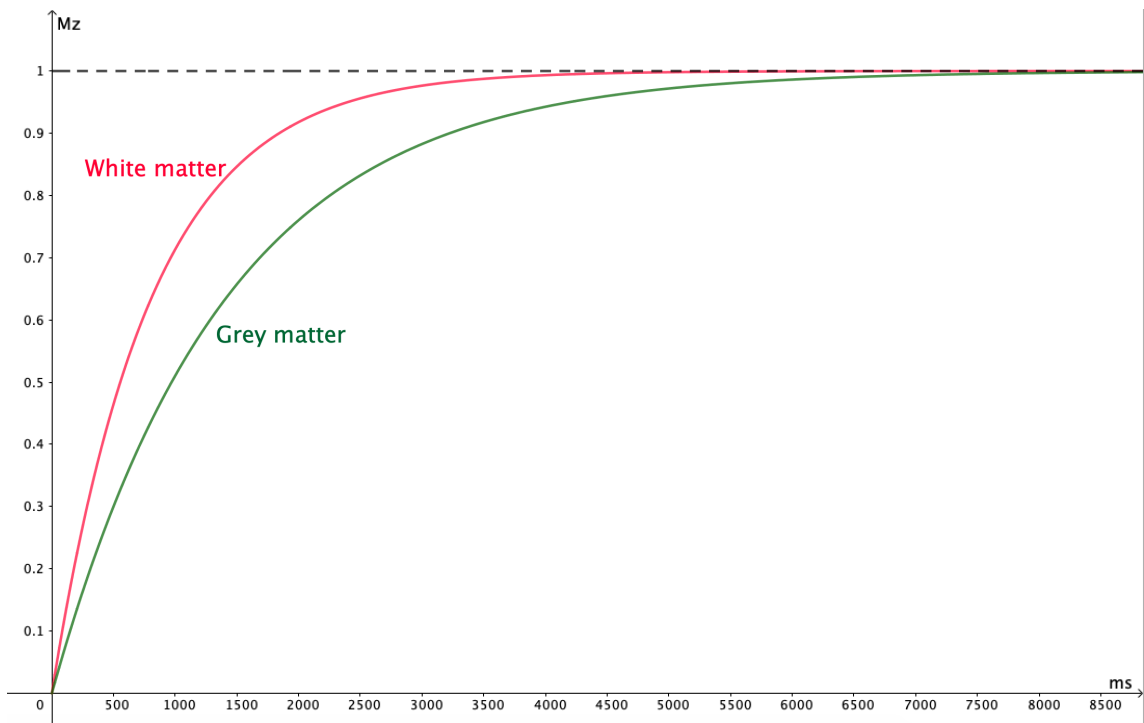


**Figure 39:** After excitation, the restoration of longitudinal magnetization in grey matter compared to white matter.

As for their  $T_2$  relaxation, in a 1999 study[31], in a 3.0T field, the grey matter had a  $T_2$  relaxation time of 110ms, while the  $T_2$  of white matter was 80ms. The  $T_2$  relaxation of grey and white matter can be seen in [Figure 40].

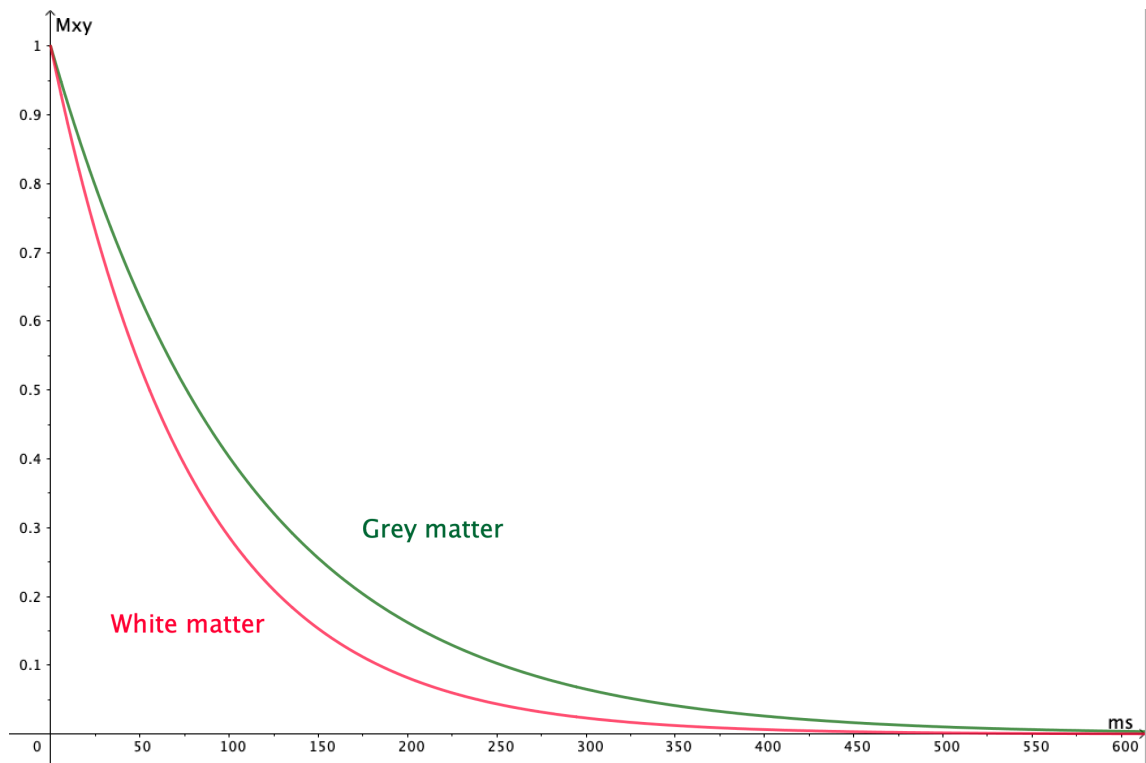


**Figure 40:** The decay of transverse magnetization in grey and white matter. The white matter with a  $T_2$  of 80ms, and the grey matter has a  $T_2$  of 110ms.

## 5 Conclusion

This thesis provided an overview of MRI hardware, image formation, basic principle physics of MR, and the most common MR contrast. MRI scanners have considerably evolved since the first commercial units were introduced to the biomedical imaging markets in the 1980s. The MRI systems are now equipped with stronger magnetic fields from high field to ultra-high-field (7 Tesla and beyond), stronger gradients, efficient RF amplifiers, advanced cooling systems, and powerful computers to reconstruct volumetric MR raw data in a short time. These advances have enabled researchers to explore the human body with more outstanding capabilities. In particular, brain research and neuroscience can gain significantly by scanning at ultra-high-field, which provides higher SNR and higher spatial and temporal resolutions.

In this work, the behavior of protons under the influence of magnetic fields has been described and visualized with the help of computer simulations written in Python, assisted by the FFmpeg extension. The simulations included the excitation and relaxation of different tissues such as grey matter, white matter, CSF, and fat. The difference in relaxation times between the tissues has been accentuated by relaxing protons from different tissues simultaneously in the same simulation. The trajectory and change in magnetization can be calculated and predicted by the Bloch equations as described in chapter 4.

How the techniques and physics behind MRI help in clinical environments have also been highlighted. It has been shown why the imaging tool is the golden standard in clinical imaging with its capability to diagnose and help treat diseases and injuries, all with little to no risks.

Today, MRI systems are essential tools in hospitals. This complex machine dive deep into the human knowledge of theoretical physics and mathematics application to humans. Historically, with the first application of the MR phenomena on a human in 1977, the MR machine is a relatively new invention. Different hardware and software related to MRI systems have been continuously improved within the past decades. Clinical imaging with magnetic resonance may be considered one of the most important and influential developments in the 1900s. The influence of the technique continues to grow 76 years after discovery[32]. Starting at a low field strength, the clinical application of MRI has seen a steady rise toward higher magnetic field strength. The advancements in hardware and software have brought the magnets up to a field strength of 7 Tesla, with 11 Tesla field magnets recently being tested[33]. Higher-strength magnets can improve the polarization of protons, which increases the signal strength, which again creates higher quality images. A few companies are working on portable MRI to generate high-quality images for 5% of the price. Artificial intelligence technology has already found its way into almost all aspects of MR imaging, allowing more efficient and automatic image analysis and evaluations.

## List of Figures

1	The astrocytoma lesion appears as the white area in the middle of the image of the patient's brain. Case courtesy of Dr Jones, J., <i>Supratentorial pilocytic astrocytoma</i> . Case study, Radiopaedia.org[1]. . . . .	6
2	Example of an MRI system inside the examination room. From the outer to inner layers of the magnet: the main magnet, the gradient coils, the RF coils, the bore where the patient lies in examination and the magnetic field is the strongest, and a sample table in which the patient is placed onto before being rolled into the bore. Springer Nature journal content, brought to you courtesy of Springer Nature Customer Service Center GmbH[6]. . . . .	9
3	Number 1 showing a cabinet containing RF amplifiers that control the RF pulse transmission and reception, and power for the gradient coils. Number 2 is the general power supply. Number 3 is the water pump for cooling. Number 4 is the helium pump that pumps helium through the machine as a coolant. Courtesy of Allen D. Elster, MRIquestions.com[7]. . . . .	10
4	A picture showing a metal stool that has flown through the air into the bore. Photo by Moriel NessAiver via The New York Times[8]. . . . .	11
5	Showcase of Maxwell's right hand rule. $I$ indicates the direction of the induced magnetic vector field coming from a current carried through the red $B$ -lines. Image by Wikipedia contributor Jfmelero via Wikipedia[9]. . . . .	11
6	A slice of an MRI scanner with a magnetic field strength of 1.5 Tesla. The bars with dotted lines depict current-carrying coils which wrap around the bore, inducing the magnetic field. As seen in the figure, the field strength quickly diminishes with distance. Image from Perry Sprawls et al., an open-access resource[10]. . . . .	12
7	Figure (a) is a knee coil from Siemens[12]. Figure (b) is a head coil from Siemens[13]. Images credited to Siemens Historical Institute. . . . .	13
8	The birdcage RF coil design. The two circular conductive loops are the <i>end rings</i> . The loops are connected by conductive elements called <i>rungs</i> , numbering from 8 to 32. Courtesy of Allen D. Elster, MRIquestions.com[14]. . . . .	13
9	A hypothetical 6-rung birdcage coil where the current through each rung is directed inwards, marked with "x". As the peak of each of the sinusoidal currents hits, the maximum flux is induced. The boldest green arrows visualize this. First, the peak of rung 1 hits, then the peak of rung 2 hits, and so on. After the sinusoidal peak sequentially hits all rungs, a peak will hit rung 1 again, and the sequence will start over. The fluctuating magnet fields inside the coil are what induce $B_1$ . Courtesy of Allen D. Elster, MRIquestions.com[14]. . . . .	14
10	The magnetic field strength equation for each of the six rungs. The phase shift equals $\frac{2\pi}{6}$ rad between each of them. All fields are summed together into one common field $B_1$ , where the equation for this field is constant. Thus, the change $\frac{dB_1}{dt}$ over time will always equal zero. If $\frac{dB_1}{dt} = 0$ , it is homogeneous. . . . .	14
11	(a) Two simple drawings of surface coils. (b) An example of a clinical surface coil. Reprinted by permission from Springer Nature: Springer Nature, <i>La radiologia medica. Uveal melanoma: evaluation of extrascleral extension using thin-section MR of the eye with surface coils</i> , Tommaso Tartaglione et al., 2014[15]. . . . .	15
12	Gradient coils. Courtesy of Allen D. Elster, MRIquestions.com[16]. . . . .	16
13	Based on a single slice from the whole region inside the cylindrical bore, where the z-axis is parallel to the main magnetic field, the action of the different gradients is visualized. As this is essentially in two dimensions (x and y), the image shows how the field strength is varied as a function of x when the x-gradient is turned on and how it goes as a function of y when the y-gradient is turned on. The z-gradient is homogeneous over the whole region, as this gradient only runs as a function of z. The combination of the x- and y-gradient in the slice give each point a different field strength. Courtesy of Allen D. Elster, MRIquestions.com[16]. . . . .	17

14	A proton spinning about its own axis, inducing a current around its body that consequently generates a magnetic field in the direction of the magnetic moment. Credit for the image goes to David Adair, via <a href="https://www.researchgate.net">https://www.researchgate.net</a> [18].	19
15	Water molecules with two hydrogen each show the random orientations of the magnetic moments when no magnetic field is applied. If anything, the direction of the magnetic moments are decided by the collision between the nuclei. Reprinted by permission from John Wiley And Sons: John Wiley And Sons, Wiley Books. <i>Basic Principles</i> , Robin A. de Graaf., 2018[5].	20
16	A proton precessing about the direction of $\mathbf{B}_0$ (green arrow) with its magnetic moment changing according to the black dotted line. The frequency of precession is $\omega$ . <i>Precession in a magnetic field</i> by FbrG is licensed under CC BY 2.0[20].	21
17	A magnetic field $\vec{\mathbf{B}}_0$ is applied to the water molecules. The protons and their spins line up parallel or anti-parallel with $\vec{\mathbf{B}}_0$ . The angle $\alpha$ at which they precess, is random for every proton. Illustration is adapted, Reprinted by permission from John Wiley And Sons: John Wiley And Sons, Wiley Books. <i>Basic Principles</i> , Robin A. de Graaf., 2018[5].	21
18	The sum of vector $\mathbf{a}$ and $\mathbf{b}$ equals a new vector $\mathbf{a} + \mathbf{b}$ . Here no components are pointing in opposite directions. Therefore, the sum vector is bigger than both $\mathbf{a}$ and $\mathbf{b}$ . If $\mathbf{b}$ was anti-parallel to $\mathbf{a}$ with the same magnitude, then they would cancel each other out, and $\mathbf{a} + \mathbf{b}$ would be zero.	22
19	Looking like a sphere made of spikes, one spike is one magnetic moment vector. Adding together >99.9% of the magnetic moments yield zero magnetization. The remaining <0.1% will account for the total magnetization in the voxel. Illustration is adapted, Reprinted by permission from John Wiley And Sons: John Wiley And Sons, Wiley Books. <i>Basic Principles</i> , Robin A. de Graaf., 2018[5].	22
20	(a) The <0.1% of protons inducing a magnetization in the z-direction. $\mathbf{M}_0$ is undetectable as the much stronger field $\mathbf{B}_0$ points in the same direction. (b) A 90° pulse is sent into the tissue at the correct frequency, and absorbed by the precessing protons. This flips the spins leading to a rotation on the xy-plane. Illustration is adapted, Reprinted by permission from John Wiley And Sons: John Wiley And Sons, Wiley Books. <i>Basic Principles</i> , Robin A. de Graaf., 2018[5].	23
21	The left image shows the protons' magnetization just after excitation. They rotate in resonance, inducing the maximum transverse magnetization. After 200ms, 63% of the protons have phase-shifted due to some rotating faster and slower than others. This de-synchronization leads to vector components canceling each other out, which lessens the transverse magnetization to 37% of maximum. Still rotating on the transverse plane, after 1000ms (5 times T2), all protons have dephased and canceled each other out. Thus, the net magnetization after adding all magnetic moment vectors is zero. Illustration is adapted, Reprinted by permission from John Wiley And Sons: John Wiley And Sons, Wiley Books. <i>Basic Principles</i> , Robin A. de Graaf., 2018[5].	24
22	The free induction decay plot, showing the loss of transverse magnetization as a function of time.	24
23	The net magnetization equals zero in all directions after T2 relaxation. However, it grows in the z-direction as the protons emit energy into surrounding tissue and flip their spins back to equilibrium. Therefore, the net total magnetization will never be zero. Note that the longitudinal magnetization will have started regrowing before the complete loss of transverse magnetization in practice. Illustration is adapted, Reprinted by permission from John Wiley And Sons: John Wiley And Sons, Wiley Books. <i>Basic Principles</i> , Robin A. de Graaf., 2018[5].	25
24	The trajectory of $\vec{\mathbf{M}}$ relaxing back to equilibrium. Credit goes to Behrooz Fateh[21].	25

25	The magnetic field strength varies in the z-direction. An image slice with a set field strength range (frequency bandwidth) is chosen. An RF pulse of this frequency is sent into the tissue. The receiver coils are tuned to only detect signals in the frequency bandwidth, and an echo of signals from only this slice is then received. Image credit goes to Radiology Cafe via <a href="http://www.radiologycafe.com">www.radiologycafe.com</a> [22]. Radiology Cafe retains the intellectual property rights on all material from their website. . . . .	26
26	An axial slice from the brain. Slices cut in the z-direction (up-down) are considered <i>axial</i> . Images "cut" in the x-direction (sideways) are sagittal, whilst coronal images are in the y-direction (front-back). Case courtesy of Dr Gaillard, F. Normal brain (MRI). Case study, Radiopaedia.org[23]. . . . .	27
27	The slice from [Figure 26] has been frequency encoded. The frequency increases with x, enabling localization of each column. Case courtesy of Dr Gaillard, F. Normal brain (MRI). Case study, Radiopaedia.org[23]. . . . .	28
28	Case courtesy of Dr Gaillard, F. Normal brain (MRI). Case study, Radiopaedia.org[23].	29
29	Standard spin-echo sequence. The echo time TE is defined from the middle of the 90-degree excitation RF pulse to the middle of the gradient echo, which coincides with the digital-to-analog converter for data sampling. The negative gradient following the pulses are necessary to refocus signal that was dephased during excitation. RF, radiofrequency; $G_{slice}$ , slice selective gradient; $G_{freq}$ , frequency encoding gradient; $G_{phase}$ , phase encoding gradient; TE, echo time; TR, repetition time. Reprinted by permission from John Wiley And Sons: John Wiley And Sons, Wiley Books. <i>Magnetic Resonance Imaging</i> , Robin A. de Graaf., 2018[24]. . . . .	30
30	The relaxation of longitudinal magnetization in grey matter compared to white matter after excitation. . . . .	31
31	The decay of transverse magnetization in grey and white matter. The white matter with a T2 of 80ms, and the grey matter has a T2 of 110ms. . . . .	32
32	The rotating frame of reference $R = (x', y', z' = z)$ rotating about the z-axis (or $B_0$ field) at an angular velocity of $-\omega$ , pictured on top of the laboratory frame of reference. Used with permission of Springer, from <i>Electron Paramagnetic Resonance Spectroscopy</i> , Bertrand, Patrick, 2020; permission conveyed through Copyright Clearance Center, Inc.[27]. . . . .	34
33	(A) Pre-excitation of magnetic moments from 9 protons. The magnetic moments are in equilibrium parallel with $B_0$ pointing in the +z-direction. The total magnetization is longitudinal. (B): Post-excitation. A 90 degree pulse at the Larmor frequency is sent to excite and flip their spins. As this is from the rotating frame of reference and a homogeneous magnetic field is assumed, the vectors follow an arc path from the z-axis down on the xy-plane where a transverse magnetization is induced. . . . .	35
34	<b>Figure A:</b> Following excitation, the decline of the longitudinal magnetization happens. The y-axis spans [-1, 1] because of the possibility of anti-parallel spins inducing a magnetization in the -z-direction. <b>Figure B:</b> The growth of transverse magnetization as seen following excitation. . . . .	36
35	A display of how protons with a slightly different precession frequency dephase in time. Fats have a short T2 relaxation time compared to water because of more frequent spin-spin interactions pushing protons away from each other and affecting the precession frequency. . . . .	37
36	The transverse magnetization decays as a function of time. The sine component of the functions is removed to get a clearer display of the decay rate. With the T2 relaxation of 1500ms, the red CSF curve is seen decaying much slower than the green curve from fat, which has a T2 relaxation of 80ms. The graphs follow the equation of $M_{xy} = e^{-(t/T2)}$ . For fat, this equals about 0.37 after 80ms, as seen in the image. This confirms that 63% of the protons have dephased after T2 time. After approximately 5 times T2, the transverse magnetization is gone in both tissues.	38
37	From excitation to total alignment with the external magnetic field - the process of T1 relaxation in fat and CSF. The differences in relaxation times are easily seen in these four images. . . . .	39

38	The restoration of 63% of the longitudinal magnetization in fat is pointed out after 250ms. After approximately 1250ms, the fat will have fully regrown to its equilibrium. CSF has a much longer relaxation time and therefore spans out of the scope of this plot, but it follows the same curve. Both tissues follow the same equation for the curve; $M_z = 1 - e^{-t/T_2}$ . . . . .	40
39	After excitation, the restoration of longitudinal magnetization in grey matter compared to white matter. . . . .	41
40	The decay of transverse magnetization in grey and white matter. The white matter with a T2 of 80ms, and the grey matter has a T2 of 110ms. . . . .	42



## References

- [1] J Jones. Supratentorial pilocytic astrocytoma, 2013. URL <https://radiopaedia.org/cases/supratentorial-pilocytic-astrocytoma>. Retrieved May, 2022.
- [2] Maudsley AA Mansfield P. Medical Imaging by NMR. *Br J Radiol.*, 50(591):188–194, 1977 Mar. doi: 10.1259/0007-1285-50-591-188.
- [3] Kyle R. A. Steensma D. P. Shampo, M. A. Nobel Prize for nuclear magnetic resonance spectroscopy. *Mayo Clin Proc.*, 87(12):e109, 2012. doi: <https://doi.org/10.1016/j.mayocp.2012.01.023>.
- [4] ML Lauzon. *A Beginner’s Guide to Bloch Equation Simulations of Magnetic Resonance Imaging Sequences*. PhD thesis, University of Calgary, 2009.
- [5] R De Graaf. *In Vivo NMR Spectroscopy: Principles and Techniques*, chapter 1. Basic Principles. .
- [6] Suraj D Serai. Basics of magnetic resonance imaging and quantitative parameters t1, t2, t2\*, t1rho and diffusion-weighted imaging. *Pediatric Radiology*, 52(2):1–11, 2022. doi: 10.
- [7] Allen D. Elster. Specifications for gradients, 2015. URL <https://www.mriquestions.com/mr-system-layout.html>. Retrieved March, 2022.
- [8] Karen Weintraub. Do m.r.i. scans cause any harm? *The New York Times*, 2017.
- [9] Wikipedia contributor Jfmelero. Right-hand rule, 2008. URL [https://en.wikipedia.org/wiki/Right-hand\\_rule](https://en.wikipedia.org/wiki/Right-hand_rule). Retrieved February, 2022.
- [10] Perry Sprawls. *Magnetic Resonance Imaging*, chapter 2. Medical Physics Publishing, 2000.
- [11] Will Morton. As mri strength increases, so do concerns about magnet safety. *Physics in Medicine Biology*, 2021.
- [12] Siemens Historical Institute. Tx/rx cp head coil, . URL <https://www.siemens-healthineers.com/no/magnetic-resonance-imaging/options-and-upgrades/coils/tx-rx-cp-head-coil>. Retrieved March, 2022.
- [13] Siemens Historical Institute. Tx/rx 15-channel knee coil, . URL <https://www.siemens-healthineers.com/pt/magnetic-resonance-imaging/options-and-upgrades/coils/tx-rx-15-channel-knee-coil>. Retrieved March, 2022.
- [14] Allen D. Elster. Birdcage coils, 2015. URL <https://mriquestions.com/birdcage-coil.html>. Retrieved March, 2022.
- [15] Monica Tartaglione, Tammaso Pagliara. Evaluation of extrascleral extension using thin-section mr of the eye with surface coils. *La Radiologia Medica*, 119(10), January 2014. doi: 10.1007/s11547-014-0388-x.
- [16] Allen D. Elster. Gradient coils, 2015. URL <https://mriquestions.com/gradient-coils.html>. Retrieved March, 2022.
- [17] Allen D. Elster. Specifications for gradients, 2015. URL <https://mriquestions.com/gradient-specifications.html>. Retrieved March, 2022.
- [18] David Adair. *Computer-assisted Screening of Motion Artefact for Quality Control in Large-scale MR Imaging Trials*. PhD thesis, The University of Calgary, 2017.
- [19] Larmor J. LXIII. On the theory of the magnetic influence on spectra; and on the radiation from moving ions. *Phil Mag*, 44(271):503–512, 1897.
- [20] Wikipedia contributor FbrG. Larmor precession, 2021. URL [https://en.wikipedia.org/wiki/larmor\\_precession](https://en.wikipedia.org/wiki/larmor_precession). Retrieved February, 2022.

- [21] Behrooz Fateh. Modeling, simulation and optimization of a microcoil for mri-cell imaging. Master's thesis, University of Rostock, 2006.
- [22] Sarah Abdulla. Larmor precession, 2021. URL <https://www.radiologycafe.com/frcr-physics-notes/mr-imaging/slice-selection/>. Retrieved May, 2022.
- [23] F Gaillard. In vivo nmr spectroscopy: Principles and techniques, 2015. URL <https://radiopaedia.org/cases/normal-brain-mri-6>. Retrieved May, 2022.
- [24] R De Graaf. *In Vivo NMR Spectroscopy: Principles and Techniques*, chapter 4. Magnetic Resonance Imaging. .
- [25] Rinck P.A. Jones R.A. et al. Torheim, G. A simulator for teaching mr image contrast behavior. *MAGMA* 2, pages 515–522, 1994. doi: <https://doi.org/10.1007/BF01766086>.
- [26] Andrew Heinzman. What is a gif, and how do you use them? URL <https://www.howtogeek.com/441185/what-is-a-gif-and-how-do-you-use-them/>. Retrieved May, 2022.
- [27] Belorizky E. and Fries P.H. *Electron Paramagnetic Resonance Spectroscopy*, chapter 10. EDP Sciences/ Grenoble Sciences; Springer International Publishing, 2020.
- [28] Clement Acquitter François Brunotte Paul M. Walker Alain Lalande Jorge Zavala Bojorquez, Stéphanie Bricq. What are normal relaxation times of tissues at 3 T? *MRI*, 25:69–80, 2017.
- [29] Frederiksen J. Petersen J. Nordenbo A. Zeeberg I. Henriksen O. Larsson, H.B.W. and J. Olesen. Assessment of demyelination, edema, and gliosis by in vivo determination of T1 and T2 in the brain of patients with acute attack of multiple sclerosis. *Magn. Reson. Med.*, 11:337–348, 1989. doi: <https://doi.org/10.1002/mrm.1910110308>.
- [30] John Huston Sean Fain Chen Lin, Matt Bernstein. Measurements of t1 relaxation times at 3.0t: Implications for clinical mra. *Proc. Intl. Soc. Mag. Reson.*, 2001.
- [31] Dunn RS Ball WS Jr. Wansapura JP, Holland SK. NMR relaxation times in the human brain at 3.0 tesla. *J. Magn. Reson. Imaging*, 9(4):531–8, 1999. doi: [10.1002/\(sici\)1522-2586\(199904\)9:4<531::aid-jmri4>3.0.co;2-l](https://doi.org/10.1002/(sici)1522-2586(199904)9:4<531::aid-jmri4>3.0.co;2-l).
- [32] Sox HC Jr Fuchs VR. Physicians' views of the relative importance of thirty medical innovations. *Health Aff (Millwood)*, 20(5):30–42, 2001. doi: <https://doi.org/10.1377/hlthaff.20.5.30>.
- [33] The iseult 11.7 t high magnetic field system for the neurospin platform, 2019. URL [https://irfu.cea.fr/en/Phocea/Vie\\_des\\_labos/Ast/ast\\_visu.php?id\\_ast=3377](https://irfu.cea.fr/en/Phocea/Vie_des_labos/Ast/ast_visu.php?id_ast=3377). Retrieved May, 2022.